NASA CONTRACTOR
REPORT

NASA CR-61375

ATTITUDE CONTROL SYSTEMS FOR LOAD RELIEF OF SATURN-CLASS LAUNCH VEHICLES

By Jerry Sharp
Northrop-Huntsville
Electro-Mechanical Division
Huntsville, Alabama 35812

February 1971

Prepared for

NASA-GEORGE C. MARSHALL SPACE FLIGHT CENTER
Marshall Space Flight Center, Alabama 35812

TECHNICAL REPORT STANDARD TITLE PAGE

1. REPORT NO.	2. GOVERNMENT ACCESSION NO.	3. RECIPIENT'S CATALOG NO.
NASA CR-61375		

4. TITLE AND SUBTITLE	5. REPORT DATE
ATTITUDE CONTROL SYSTEMS FOR LOAD RELIEF OF SATURN-CLASS LAUNCH VEHICLES	February 1972
	6. PERFORMING ORGANIZATION CODE
7. AUTHOR(S) Jerry Sharp	8. PERFORMING ORGANIZATION REPORT #
9. PERFORMING ORGANIZATION NAME AND ADDRESS Northrop-Huntsville Electro-Mechanical Division Huntsville, Alabama	10. WORK UNIT NO.
	11. CONTRACT OR GRANT NO. NAS8-20082
12. SPONSORING AGENCY NAME AND ADDRESS NASA Washington, D. C. 20546	13. TYPE OF REPORT & PERIOD COVERED Contractor Report
	14. SPONSORING AGENCY CODE

15. SUPPLEMENTARY NOTES

Technical Coordinator: John Livingston, Dynamics and Control Division, Aero-Astrodynamics Laboratory, George C. Marshall Space Flight Center, Alabama 35812

16. ABSTRACT

This report presents the results of a study of the effectiveness of attitude control laws that are designed to reduce bending moment loads and improve the controllability of large Saturn class boosters. These laws are referred to as load relief control systems within this report. The two factors are assessed by simulations of varying degrees of complexity, from 2-D rigid body to 6-D with flexible body. A load relief control system, nicknamed AGE, is selected as the most effective of the various proposed schemes. This system is compared with other load relief laws and with simple attitude control. Most nominal vehicles use attitude control laws since their goal is to stay on the flight path without regard to the induced loads.

17. KEY WORDS	18. DISTRIBUTION STATEMENT
Bending Moment loads Attitude Control laws	Unclassified-Unlimited E. D. GEISSLER Dir, Aero-Astrodynamics Lab, MSFC

19. SECURITY CLASSIF. (of this report)	20. SECURITY CLASSIF. (of this page)	21. NO. OF PAGES	22. PRICE
Uncl	Uncl	80	$3.00

MSFC - Form 3292 (May 1969)

SUMMARY

This report evaluates the effectiveness of several proposed load relief control laws and selects a candidate control law that promises to best relieve bending moment loads while holding dispersions to a minimum.

Saturn class vehicles are capable of lifting very large payloads into earth orbit. However they are usually limited by bending moment loads to payloads smaller than their propulsive capability. The principal in-flight disturbance is wind and wind induces the severest bending moments on the vehicle other than those caused by mechanical failures.

Since the vehicles considered in this report are aerodynamically unstable during most or all of their boost stage, they tend to head away from the wind with simple attitude control systems, a situation that increases bending moments and reduces controllability. Therefore the load relief control laws examined in this report all have one thing in common. They act to turn the vehicle into the wind.

Simulation of the various vehicles with the proposed control systems enables the investigator to choose the scheme that best alleviates the flight problem of the particular booster, whether it is excessive bending moments or uncontrollability, or both. Using mostly rigid body simulations, a control law (AGE) was devised that appears to best meet both of these problems. After the rigid body effects were assessed, the flexible body effects were examined by simulation programs and stability tools such as closed loop eigenvalue calculations, root locus, nyquist and Bode plots. The AGE control law appears to pass all these tests satisfactorily. Flexible body effects have been examined in full detail on some of the configurations and preliminary filters are included to stabilize the feedback channels.

TABLE OF CONTENTS

LIST OF ILLUSTRATIONS

LIST OF TABLES

DEFINITION OF SYMBOLS

ENGLISH

Symbol	Definition
a_o	attitude feedback gain
a_1	attitude rate feedback gain
AC	attitude error plus attitde error feedback or attitude control
AGE	attitude rate plus lateral body-axis acceleration and reference axis velocity feedback
C_{M_α}	aerodynamic moment coefficient
C_{N_α}	aerodynamic force coefficient
C_1	$Q\ C_{M_\alpha}/I_y$
C_2	$R'\ \bar{x}_E/I_y$
D_o	reference diameter
e_1	velocity feedback gain
F_T	total axial thrust
F_x	total axial drag
g_2	body accelerometer feedback gain
I_E	moment of inertia of movable engines
I_y	moment of inertia of vehicle about y-axis
k_E	length from engine c.g. to engine gimbal point
K_1	$(F_T - F_x)/M = \ddot{x}$
K_2	$Q\ C_{N_\alpha}/M$
K_3	R'/M
M	mass of vehicle
M_{B_i}	modal mass of i^{th} bending mode

DEFINITION OF SYMBOLS (Continued)

ENGLISH

Symbol	Definition
M_E	mass of movable engines
M_{sj}	mass of j^{th} slosh mode
M'_α	angle of attack bending moment coefficient
M'_β	engine deflection angle bending moment coefficient
q	dynamic pressure
Q	$\frac{\pi q D_o^2}{4}$
R'	vectorable thrust
V	velocity along trajectory
V_W	wind velocity
x	missile body axis (positive forward)
X	displacement along missile reference axis (positive forward)
x_{cg}	missile body station of center of gravity
x_{cp}	missile body station of center of pressure
x_E	missile body station of engine gimbal
x_g	missile body station of attitude gyro
x_{Rg}	missile body station of rate gyro
$\bar{x}_{cp}$	$x_{cg} - x_{cp}$
$\bar{x}_E$	$x_{cg} - x_E$
y	missile body axis
Y	displacement along missile reference axis
$y_i(x)$	normalized bending displacement at station (x) of i^{th} mode

DEFINITION OF SYMBOLS (Concluded)

ENGLISH

Symbol	Definition
$y_i'(x)$	slope of normalized displacement at station (x) of i^{th} mode
z	missile body axis
Z	displacement along missile reference axis
$\ddot{z}_a$	acceleration along the z-axis sensed by body mounted accelerometer
$\dot{Z}_p$	velocity at station p along the Z-axis
$\dot{Z}_R$	lateral reference-axis translation

GREEK

α	rigid body angle of attack
α_w	angle of attack due to wind
β	engine deflection angle
β_c	engine deflection command
$\hat{\beta}_c$	engine force command
ξ_E	engine quadratic damping
ξ_i	damping of i^{th} bending mode
η_i	generalized bending mode coordinate
ϕ	rigid body yaw attitude error
$\dot{\phi}$	rigid body yaw attitude rate
ϕ_g	attitude gyro output
$\dot{\phi}_{Rg}$	rate gyro output
ω_D	drift root
ω_E	natural frequency of engine quadratic
ω_i	natural frequency of i^{th} bending mode
ω_N	natural frequency of rigid body

Section I

INTRODUCTION

Since 1965 Northrop has been performing research and studies on load relief control systems for large Saturn class boosters. This work was done under Contracts NAS8-20082 and NAS8-11111. This report presents the results of the most recent of these investigations.

The objective of these studies has been to design a load relief control system that will give a significant reduction of inflight loads and alleviate any controllability problems the flight vehicle might have; yet the candidate system must also be feasible when the booster's flexible body motions are included. Each vehicle is a new problem but since flight dynamics are similar between the vehicles, the load relief control law turns out to be about the same for each vehicle.

The results of the analysis of several vehicles are presented in this report. These vehicles are shown on Figure 1-1. In order, they are: the familiar Saturn-V Apollo launch vehicle; the Saturn-IB powered Wet Workshop, which was replaced while still in design by the Skylab concept; the Saturn-V powered Skylab, due to fly in 1972-73; and finally the proposed Intermediate-21 space station launcher, which has several possible payload lengths. The particular load problems of each of these vehicles will be explained in its own section.

Basically there are three ways to reduce loads in vehicles that are aerodynamically unstable during most of their flight time. Management can accept reduced launch availability and plan no flights during months that have predicted wind envelopes above a certain velocity and/or with an expected occurrence rate greater than some limiting value. An obvious drawback to this plan occurs when planned missions to assemble space stations in orbit are considered. Reduced launch access makes it difficult to plan and carry out the assembly of the modules on a preset schedule. Delays would impact crew supply and increase launch costs.

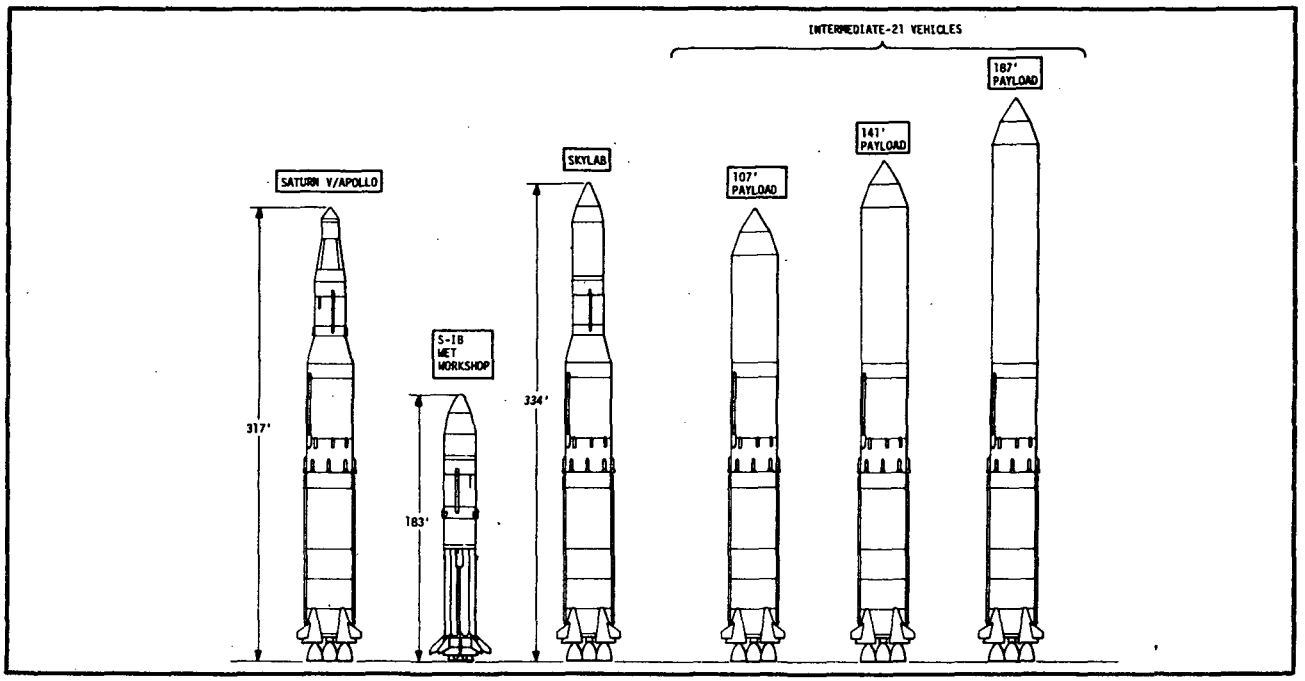

Figure 1-1. VEHICLES EXAMINED IN REPORT

The second load relief procedure is wind biasing. Pitch plane wind biasing now used on Saturn/Apollo flights and has proved successful in the past. However, the S-IC has the least severe load problem of any of the other vehicles under this study and some of the other configurations don't receive enough load relief from wind biasing to achieve a suitable launch availability. Furthermore, the wind biasing depends on accurate statistical prediction of the expected wind, since current launch rules require the biasing program to be programmed several months before the flight.

The third method, and the technique presented in this report, is active load relief using a load relief control system. The control system is designed to turn the booster into the wind to reduce loads. Two different kinds of sensors can create this effect, accelerometers and angle-of-attack meters. Results have shown that these two sensors give equivalent rigid body responses (ref. 12).

Allowing the vehicle to turn into the wind reduces the angle-of-attack. This in turn increases the controllability since the control system is not trying to hold the vehicle to some preset, open loop programmed, attitude angle. Since the bending moment is calculated from equation (1) it too will be reduced if the load relief control system does its work well.

$$BM(\alpha, \beta, \ddot{\eta}_i, X) = M'_\alpha(X) * \alpha + M'_\beta(X) * \beta + \sum_{i=1}^{n} M'_{\ddot{\eta}_i}(X) * \ddot{\eta}_i \qquad (1)$$

The M' are the bending moment partials with respect to angle-of-attack (α), gimbal angle (β), and flexible body mode acceleration ($\ddot{\eta}_i$).

The only terms not obviously reduced by the load relief control law are those that depend on $\ddot{\eta}_i$. The text of the report attempts to assess the impact of these variables as well as angle-of-attack and gimbal angle. In general the results show that the effect of the bending vibrations is not enough to drastically change the bending moment comparisons, and of course the vibrations don't appreciably change the gimbal angle requirements.

For the most part, only two control laws are used. The first, the "drift minimum" law, was originally designed to reduce drift on the Saturn I-B, a by-product being reduced loads. This system feedback paths are shown in Figure 1-2.

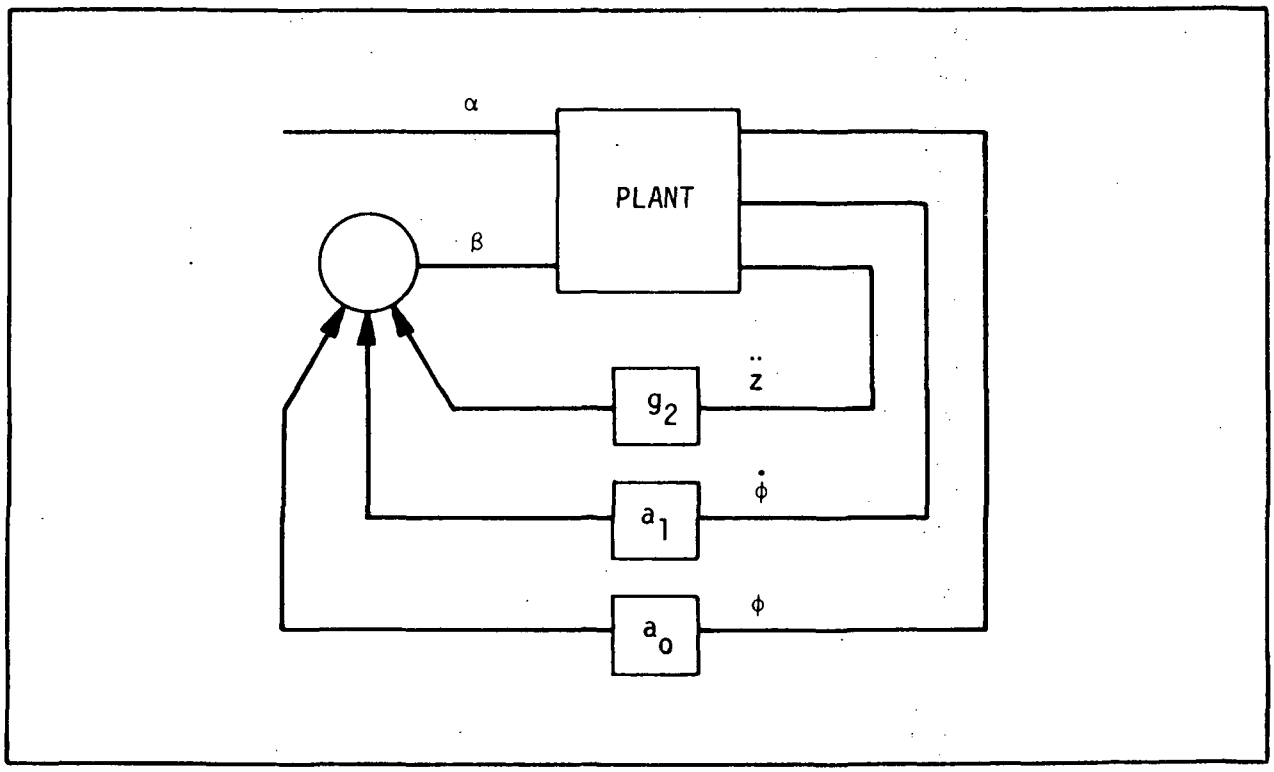

Figure 1-2. DRIFT MINIMUM SYSTEM

A three-gain system like the drift minimum system allows the analyst to specify the system closed loop natural frequency (ω_n), the damping ratio (ζ), and the drift root*(ω_D). It is shown in this report that allowing ω_D to get large increases the load reduction. This may cause some confusion in the nomenclature since the original drift minimum system was so named because ω_D was forced to zero. Perhaps a better name would be free drift or AAG (for a_0, a_1, g_2) but drift minimum is the original name.

The other load relief law is called AGE (for a_1, g_2, e_1). A block diagram of the feedback path is shown in Figure 1-3.

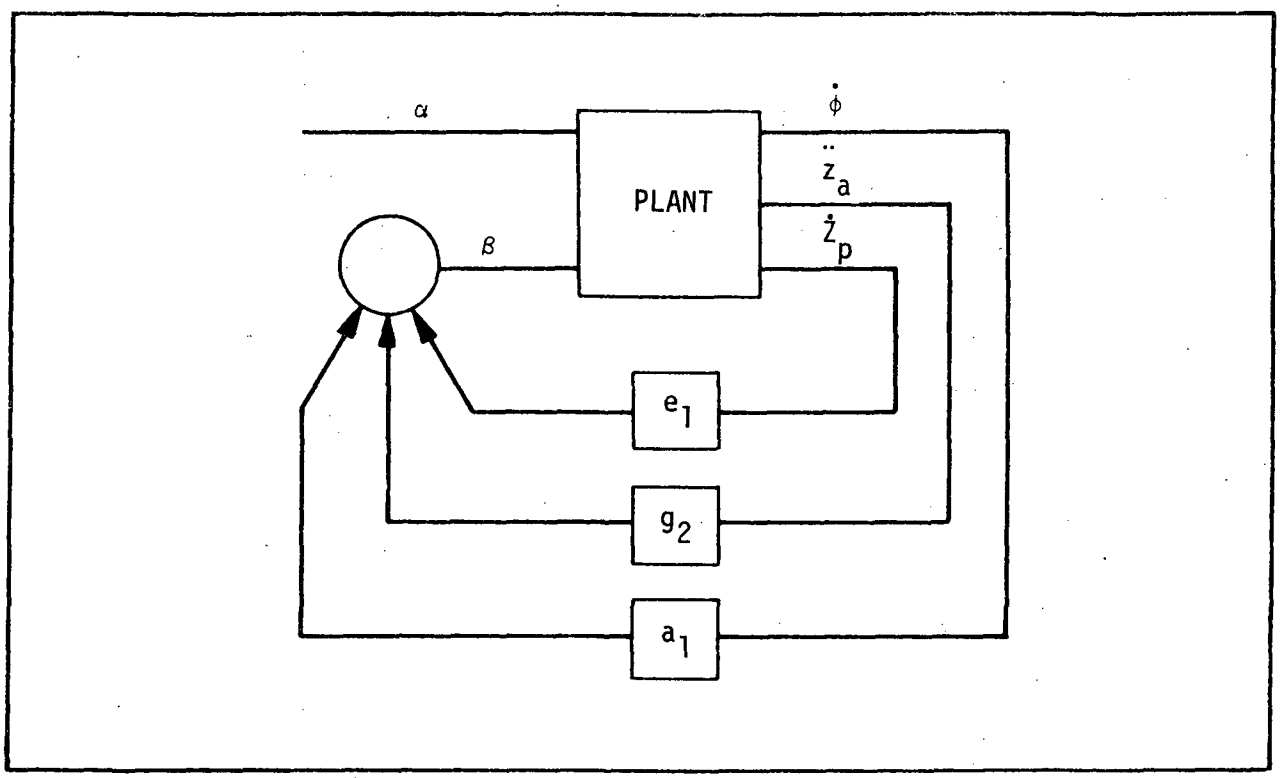

Figure 1-3. AGE SYSTEM

Again, since there are three gains, the investigator may specify (ω_n, ζ, ω_D) to any values within the realizable range. Results presented later in this report show that ω_D is not as powerful an influence on loads as it is in drift minimum. It is maintained that the success of AGE stems from the lack of any attitude reference at all.

* *The drift root is an eigenvalue of the characteristic matrix that represents the drift velocity from the nominal trajectory.*

Regardless of the load relief control law, it is only used during the high q region of flight. The actual times depend on the vehicle and its trajectory. Load relief is not needed during the remainder of flight and there are drawbacks to load relief during lift-off or near the end of flight. During lift-off, a load relief control law will have tower clearance problems. Near the end of first stage flight the Saturn I-C has an attitude freeze in order to avoid interfering with the second stage iterative guidance and to remove transients before separation. Any load relief system would be unsuitable for this attitude freeze.

A typical gain schedule, as used in the report, is shown in Figure 1-4. The gains are ramped in and out to avoid large artificial transients in the control system.

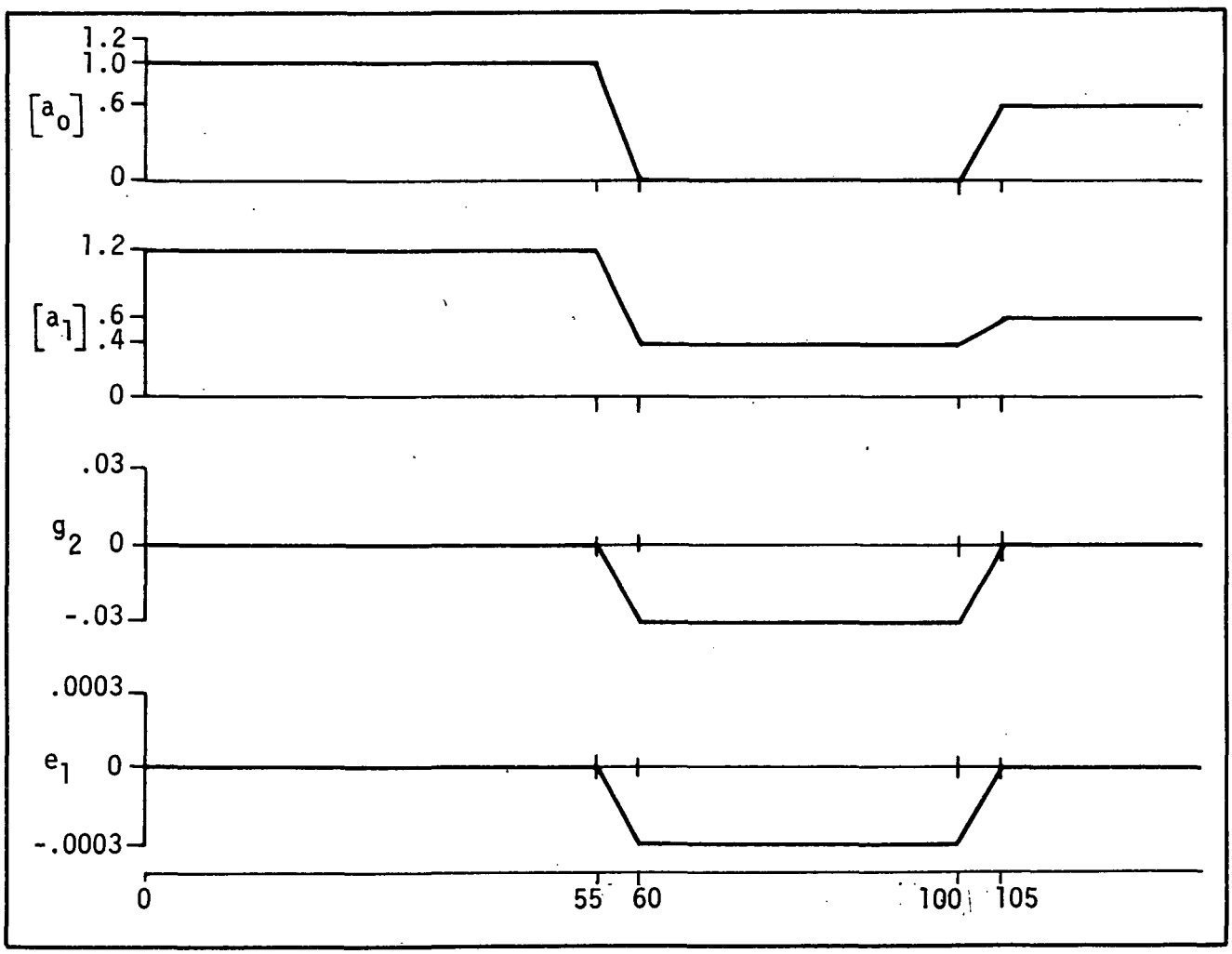

Figure 1-4. CONTROL GAIN SCHEDULE FOR THE PROPOSED S-IC AGE SYSTEM

Section II
MATH MODELS

2.1 EQUATIONS OF MOTION

Most of the work in this study was done using a perturbation program having two degrees of rigid body freedom and two bending modes. These equations are assembled in Figure 2-1 and programmed on an EAI 690 hybrid computer. This simple model was used for a good percentage of the work, but two other simulation tools were used when a more detailed examination of some of the phenomena was required. One of these simulations included a full six-degree-of-freedom and the other had five-degrees-of-freedom (no roll) with flexible body effects (a hybrid program on the EAI 8900).

The principal investigative tool is the EAI 690 2-D program. It has the capability for second-order servo, nonlinear aerodynamics and filters along with the two degrees of rigid body freedom and two bending modes.

The EAI 8900 system is a hybrid system with two main components. The EAI 8800 analog computer was hooked in a dual patchboard mode with each patchboard having 60 integrators, 60 summers, 80 inverters (18 of which function as multipliers), and 220 servo-set potentiometers. This system was interfaced with an 8400 digital computer with 32 parallel D/A conversion channels.

The EAI 690 also has two main components. The EAI 680 analog computer is equipped with 30 integrators, 24 summers, 90 inverters, various function generators and comparators and 120 servo-set potentiometers. It is coupled by 24 A/D trunks and 12 D/A trunks to the EAI 640 digital computer.

2.2 WIND

The greatest cause of loads during the boost phase of flight is wind. For the worst case wind, this study uses an artifical wind profile based on references 15 and 16. This profile represents a March wind with magnitude equal to a greater than 95 percent of previously measured March winds and shear buildup and gust greater than an equal in severity to 99 percent of measured March values. This

$$\ddot{Z} + K_2 \alpha + K_1 \phi + \sum_{i=1}^{2} 1.25\, K_3\, Y_i'(X_E)\, \eta_i + K_3 \beta = 0 \tag{1}$$

$$\ddot{z} + K_2 \alpha + \sum_{i=1}^{2} 1.25\, K_3\, Y_i'(X_E)\, \eta_i + K_3 \beta = 0 \tag{2}$$

$$\frac{\dot{Z}}{V} + \alpha_W + \phi = \alpha \tag{3}$$

$$\ddot{\phi} + C_1 \alpha + C_2 \beta + \sum_{i=1}^{2} \left[1.25\, C_2 \left(Y_i'(X_E) - \frac{Y_i(X_E)}{X(cg)}\right) \eta_i\right] = 0 \tag{4}$$

$$m_{b_i} \left[\ddot{\eta}_i + 2\zeta_i\, \omega_i\, \dot{\eta}_i + \omega_i^2\, \eta_i\right] + \left[k_E\, m_E\, Y_i(X_E) + I_E\, Y_i'(X_E)\right]\ddot{\beta} + m\, K_3\, Y_i(X_E)\beta = 0 \tag{5}$$

$$\ddot{\beta} + 2\, \zeta_E\, \omega_E\, \dot{\beta} + \omega_E^2\, \beta = \omega_E^2\, \beta_c \tag{6}$$

$$\beta_c = a_o\, \phi_e + a_1\, F_{\dot{\phi}} \left[\dot{\phi}_p + \sum_{i=1}^{2} Y_i'(X_p)\, \dot{\eta}_i\right] + g_2\, F_{\ddot{z}} \left[\ddot{z} + \overline{X}_a\, \ddot{\phi} + \sum_{i=1}^{2} Y_i(X_a)\, \ddot{\eta}_1\right] + e_1 \left[\dot{Z} + \overline{X}_p\, \dot{\phi} + \sum_{i=1}^{2} Y_i(X_p)\, \dot{\eta}_i\right] \tag{7}$$

Figure 2-1. EQUATIONS OF MOTION

profile is shown in Figure 2-2 with a gust time at 73 seconds for an Intermediate-21 flight. Other flight times are used for the Intermediate-21 and other vehicles but the analysis is concentrated in the time near the region of maximum q or maximum $q*\alpha$ product. In general, this time is different for each vehicle.

This study also uses an example of a severe measured wind. This wind was measured on the AS-504 flight and is the worst wind a Saturn class vehicle has yet to actually experience. The wind has a changing azimuth to go with its varying magnitude so it cannot be shown on a single chart but it is used in the five-degree hybrid program. However, an idealization of this wind to the plane is shown in Figure 2-2. This wind is used in the 2-D hybrid program. Other, less severe, measured winds are also used in the 2-D studies. All these winds were picked as representative of the more severe winds a vehicle is likely to encounter in flight.

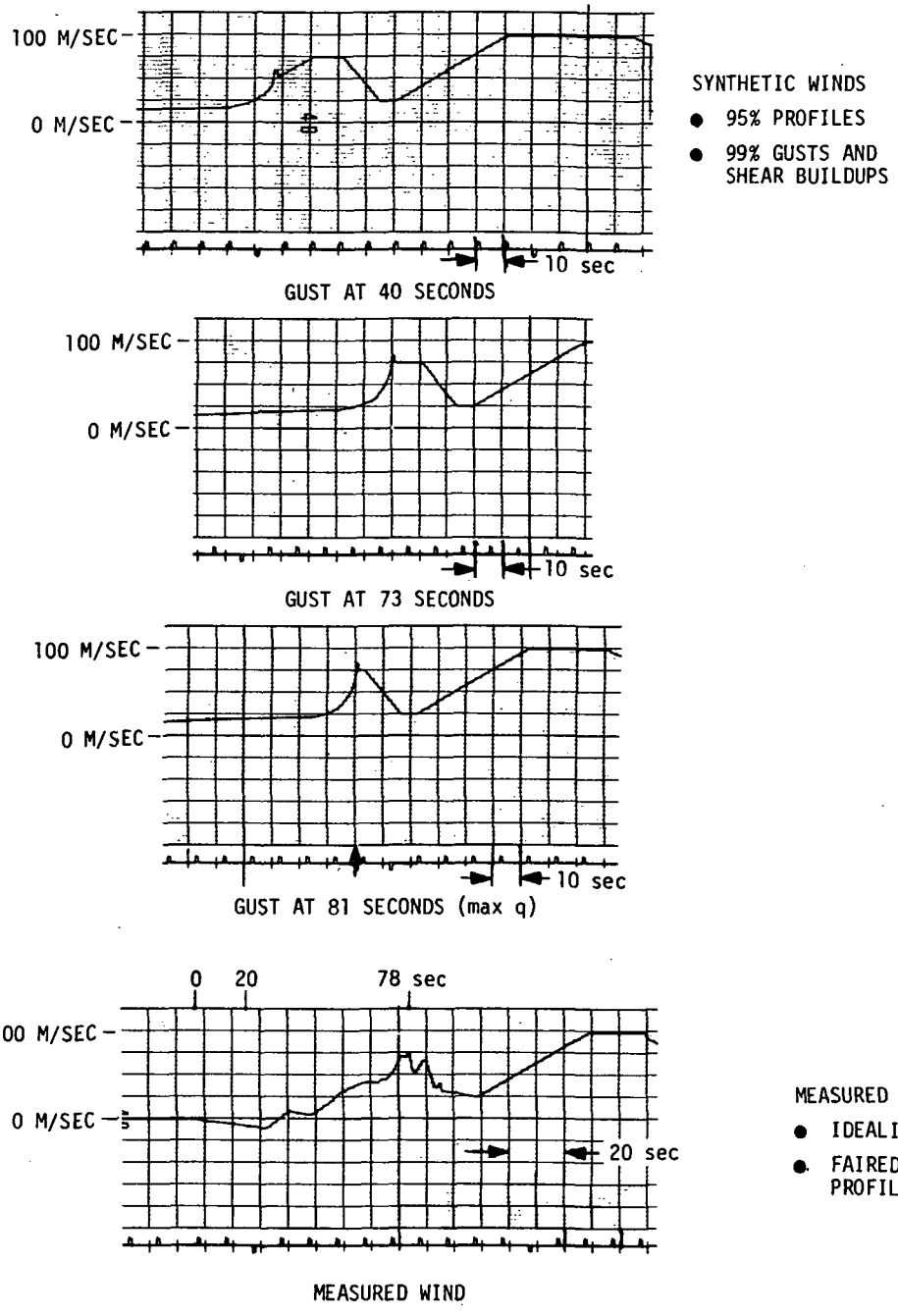

Figure 2-2. EXAMPLE WINDS USED IN INTERMEDIATE-21 STUDY

Section III
RESULTS

3.1 SATURN V/APOLLO

3.1.1 Problem Definition and Approach

Many runs were made on this configuration using the 2-D simulation with no flexible body. For this study the simulation had rigid body only. It also used linear aerodynamics, ideal filters, and ideal servo representation.

The Saturn V does not have a load problem with the current AC system. Also it has plenty of control authority with this controller. Simulation shows only about one degree of gimbal angle required to trim the vehicle in the worst case synthetic wind. However, this booster is typical in many respects and it was desired to assess the improvement attainable with a load relief control law.

The problem is approached by performing a frozen time analysis to evaluate the effects of gains and parameters. Frozen time means all vehicle parameters are set to their values at max $q\alpha$ and held there for a time slice of about 20 seconds. This gives conservative results in general but saves computer time. After the frozen time analysis is complete the variable time analysis (vehicle parameters vary with time) begins. The variable time work will show up such problem areas as control systems tuned to a certain wind and drift problems and uncover any flight regimes that the control system will give unsatisfactory performance.

3.1.2 Frozen Time Results

As a summary, Figure 3-1 shows the frozen time (FT) or frozen vehicle parameter results for the best AC, DM, and AGE systems. Frozen time runs are conservative (about 20 percent - reference 11) since the vehicle parameters are fixed at the maximum q or $q\alpha$ values. However, they are valid for comparisons. The results in Figure 3-1 are obtained by subjecting the control systems to the frozen time wind in Figure 3-2. This wind is also typical of the frozen time winds used later in the report.

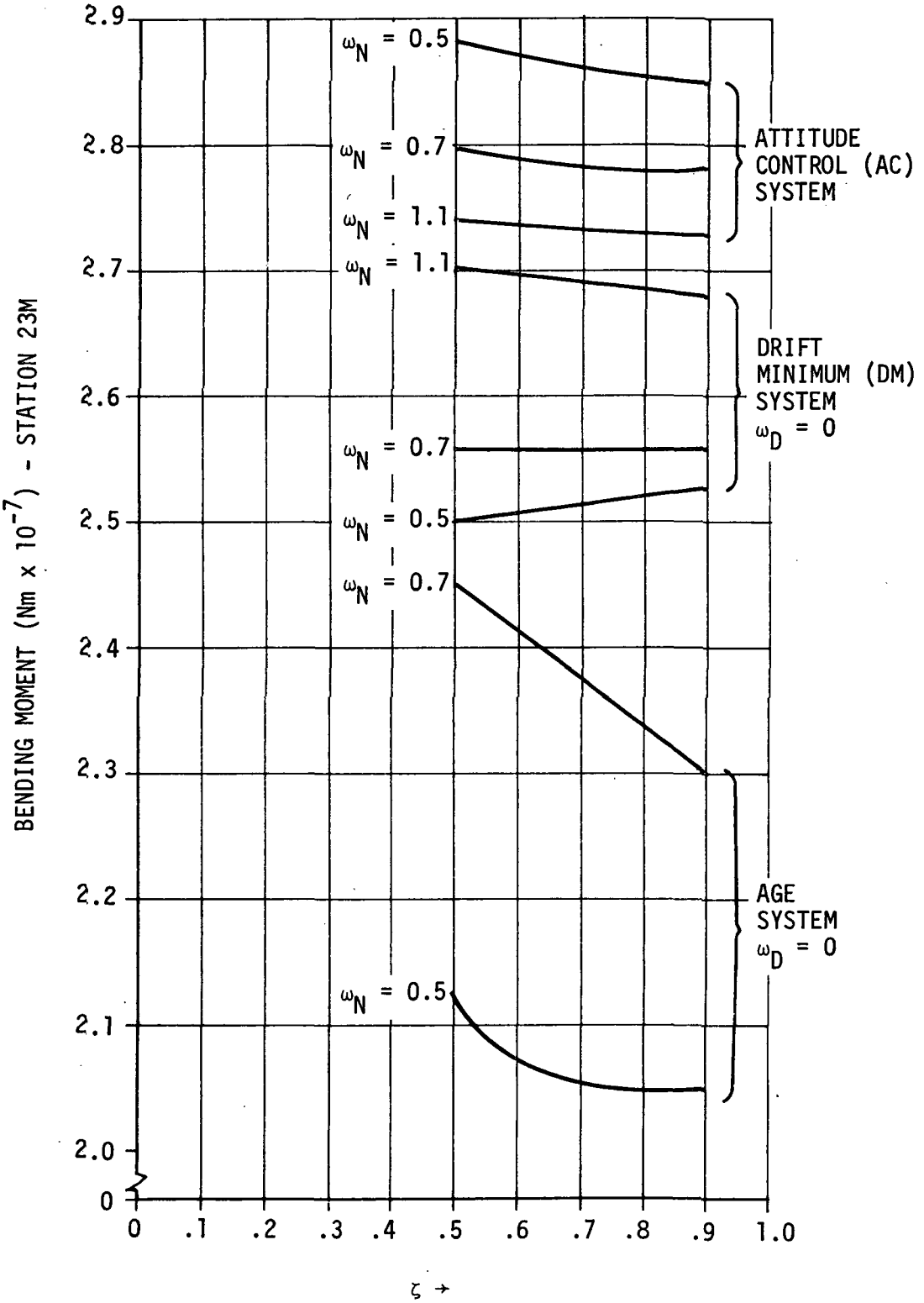

Figure 3-1. MAXIMUM BENDING MOMENT FOR AC, DM, AND AGE SYSTEM USING FT ANALYSIS

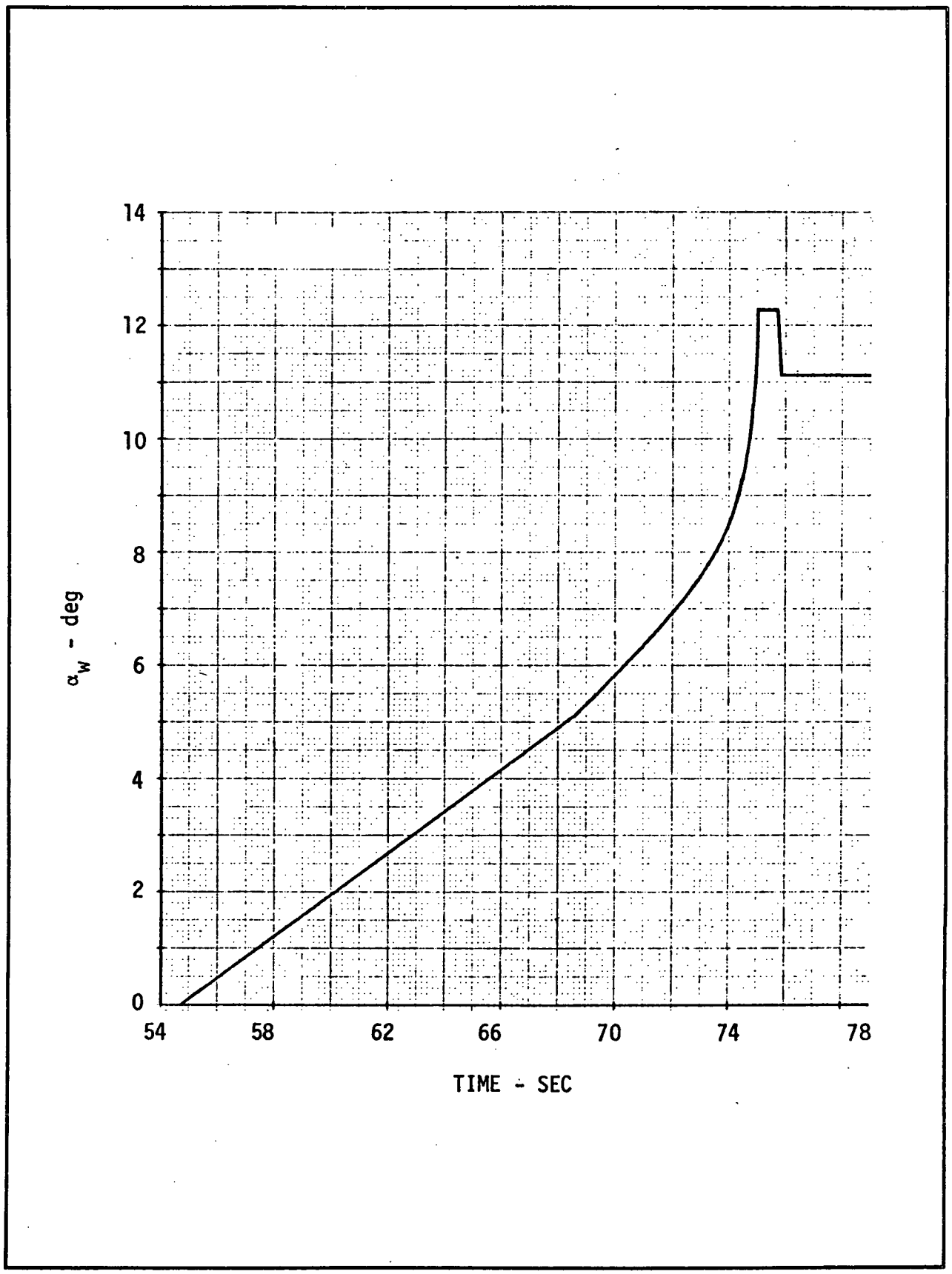

Figure 3-2. WIND USED IN FIXED TIME STUDY

Results given in reference 7 show that AGE gives slightly better bending moments (5 percent) with a non-zero drift root but the improvement must be balanced against larger transients at ramp-out and increased drifts and drift rates.

A comparison of the results reveals that the best AGE gain set ($\omega_D = 0$) reduces bending moments by about 23 percent compared to AC while DM reduces loads only about 4.5 percent. On the basis of this study, this AGE system is chosen as the load relief law for the next part of the study.

3.1.3 Variable Time Results

Nine different winds are used for this part of the study. They include three 95-percentile profiles with 99-percentile shears and gusts occurring at different flight times. One of the winds is a reverse shear with 95-percentile profile and 99-percentile shear breakoff. Five measured winds make up the remainder of the nine winds used in the study. These winds are given in reference 7.

The results of the wind study are in Figure 3-3. Configuration 1 is the reference AC system and configuration 6 is the AGE system chosen for best all around response characteristics and best reduction of bending moments. It can be seen that the bending moment reduction from AC to AGE varies about from 17 to 33 percent, with the exception of wind 8 which is a low magnitude, early peaking, measured wind. Wind 8 does not cause very high bending moments in any case.

3.1.4 Summary

In summary, an AGE control law has been shown effective in reducing in flight bending moments to a significant degree. Since controllability is not a problem on the S-IC, the increase in gimbal margin is not shown. However, the interested reader can find the comparison between gimbal angle requirements for AGE and AC in reference 7. It should be pointed out that no flexible body equations are used in this vehicle study.

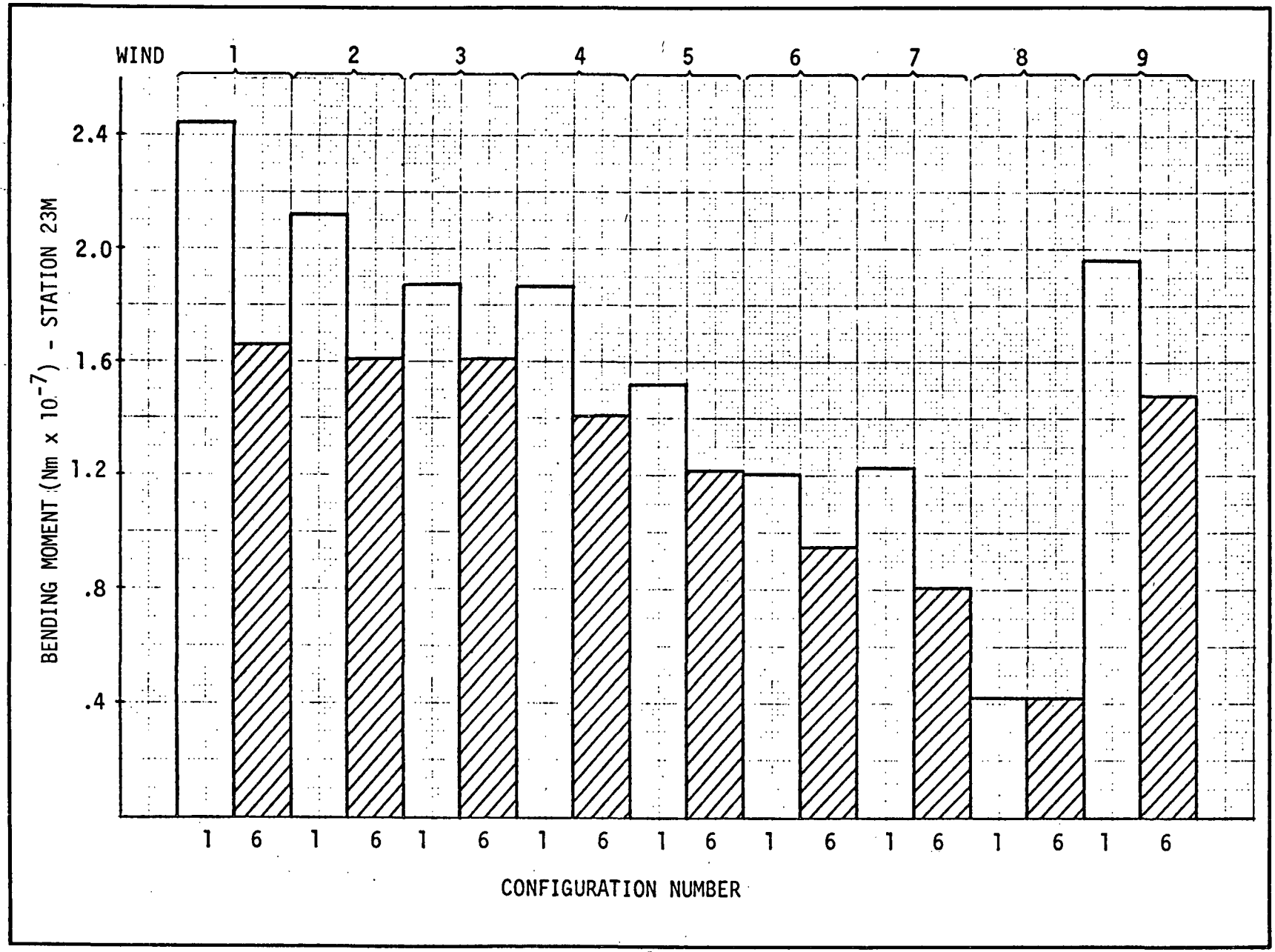

Figure 3-3. COMPARISON OF BENDING MOMENT OF ATTITUDE AND AGE CONTROL FOR SYNTHETIC AND MEASURED WINDS

3.2 SATURN IB WET WORKSHOP

3.2.1 Problem Definition and Approach

This study is done almost entirely on the 2-D simulation, which has rigid body, linear aerodynamics and no filters. The approach is similar to the S-IC study. First a frozen time analysis is made using the March worst case synthetic wind shown in Figure 3-2. Vehicle parameters are frozen at max $q\alpha$ (67.5 seconds). After the frozen time analysis points up the influence of the various parameters on bending moment, angle-of-attack, and gimbal angle, a variable time analysis is performed to further tune the gains and examine the secondary effects of the chosen control systems.

3.2.2 Frozen Time Results

The frozen time analysis is summarized in Figure 3-4. Here it can be seen that bending moment is, in general, lowest for the AGE control system, higher for the drift minimum (DM) system, and highest for the AC reference system. Figure 3-5 shows that the drift minimum control law with non-zero drift root (DMWD) falls between the drift minimum law and the AGE law, approaching the latter for increasing magnitudes of ω_D, the drift root. However, the AGE law used to give the results in Figure 3-4 has ω_D set to zero, and some reduction in peak bending moment can be gained by letting this root in the AGE law become larger.

On this configuration, just as on the S-IC booster, controllability is not a major problem. However, the engine gimbal limits are approached more closely on the S-IB than on the S-IC. To gain some idea of the controllability margin on the S-IB, consider Figure 3-6 which gives the gimbal limits and the maximum gimbal angles for AGE, DM, and AC control laws as a function of ω_n and ζ. The gimbal limits are not exceeded by any control law, even though the study is done in frozen time which gives conservative results.

Summarizing the frozen time results, we can say that both the DMWD and AGE control laws yield significant decreases in peak bending moments but one

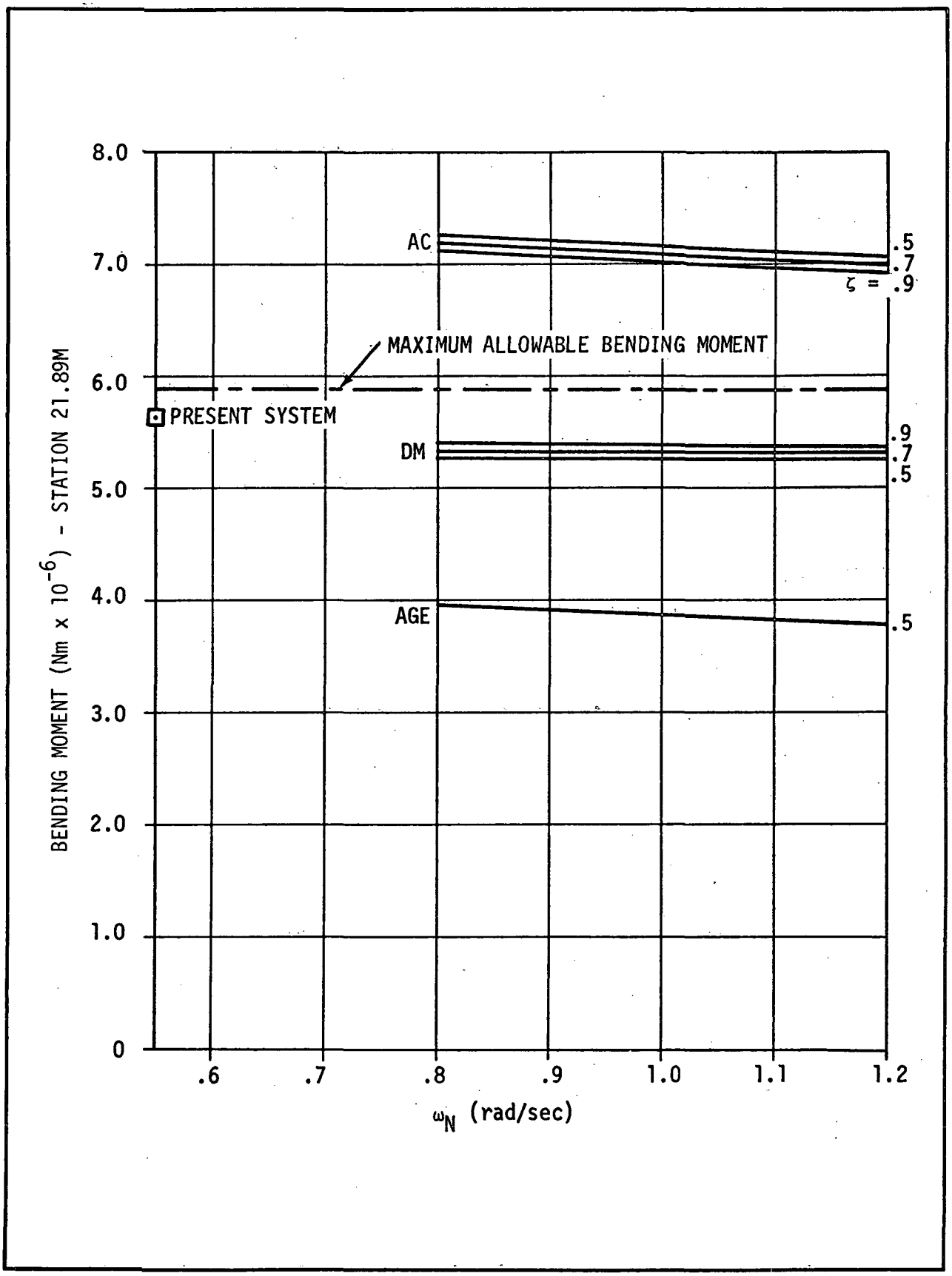

Figure 3-4. BENDING MOMENT AS A FUNCTION ω_N WITH ζ AS A PARAMETERS

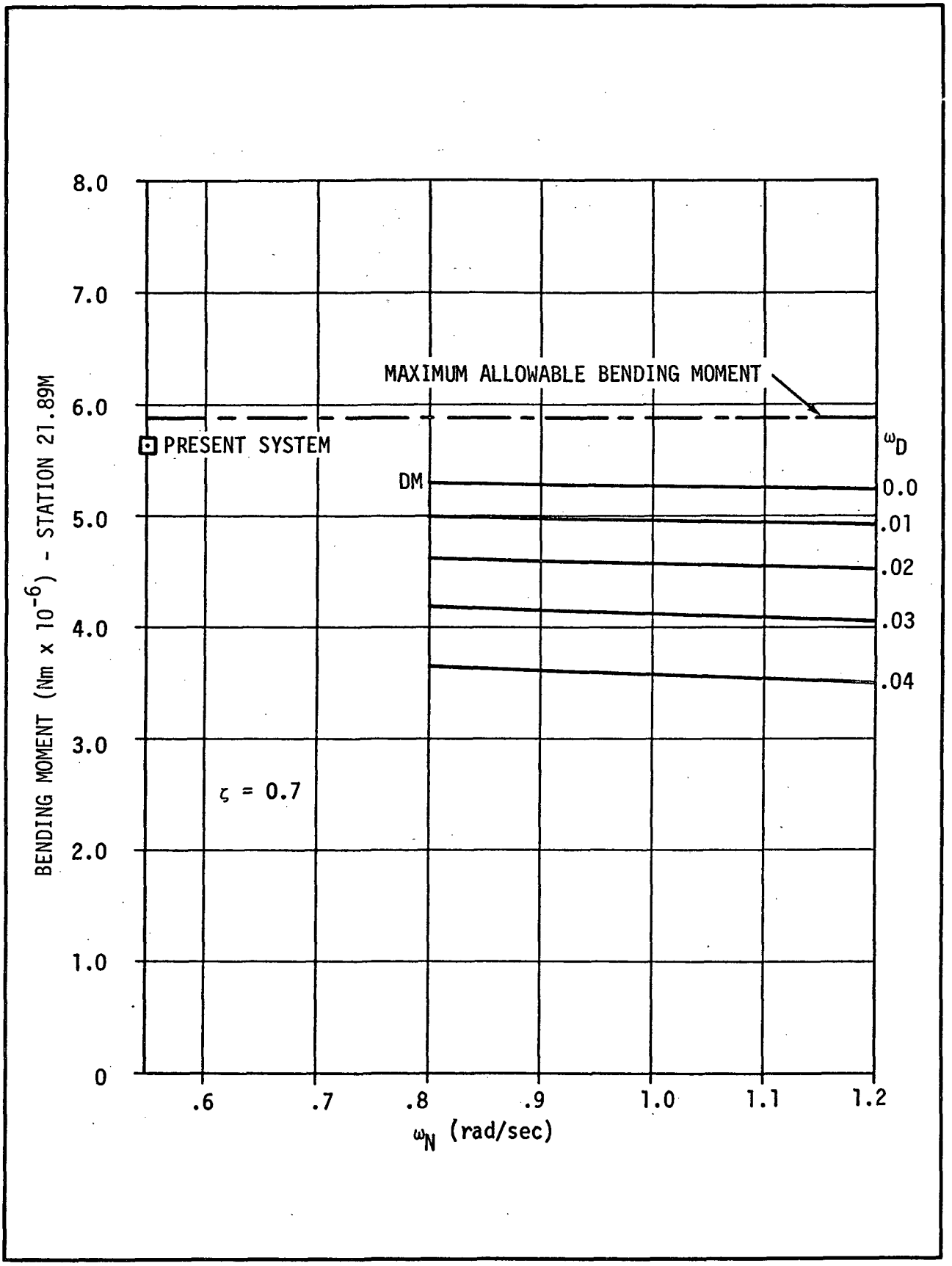

Figure 3-5. BENDING MOMENT AS A FUNCTION OF ω_N WITH ω_D AS A PARAMETER FOR THE DMWD LAW

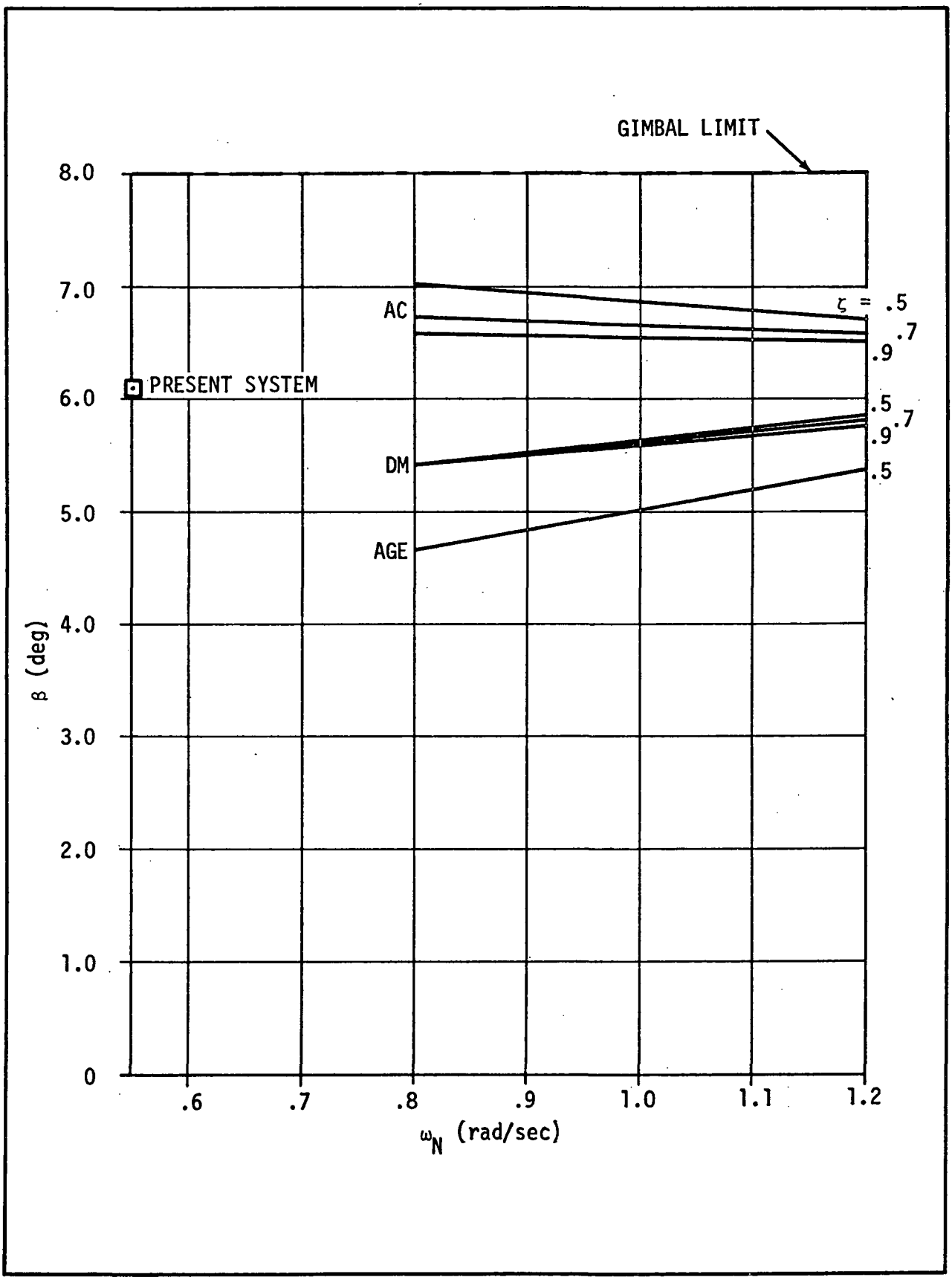

Figure 3-6. ENGINE DEFLECTION ANGLE AS A FUNCTION OF ω_N WITH ζ AS A PARAMETER

has not been demonstrated to be significantly more effective than the other. The determination of superiority must be withheld until the variable time study is completed.

3.2.3 Variable Time Results

The variable time analysis is also conducted identically to the S-IC study. Several synthetic winds are selected that peak at various times in flight. All of them have 95 percentile profiles and 99 percent shear buildups and gust magnitudes. The measured winds are the same ones mentioned in subsection 3.1.3.

One problem characteristic of any load relief control law is the buildup late in flight of α, β and bending moment. A gain schedule must be devised to minimize the late peaks while holding the wind-gust-caused peaks to an acceptable value. Often it becomes a trade-off between reduced bending moment at the wind gust and increased bending moment later in first-stage flight. The AGE gain schedule that gives the best results for this vehicle is given in Figure 3-7, along with the best choices for the DM, DMWD, and AC control laws. There is also a nominal set. For the origin of this set see below.

The results of the simulation of these control laws against synthetic and measured winds are given in Figures 3-8 and 3-9. In Figure 3-8 the control laws are compared against various 95 percent synthetic winds with gust times as shown at the bottom of each triad of control law bar graphs. The nominal entry refers to the gain set so labeled in Figure 3-7 which was used on the S-IB flights. It is essentially a drift minimum system with different gains than the DM system used for this study and was included for reference comparisons. From Figure 3-7 it can be seen that AGE decreases the maximum bending moments 13 percent to 26 percent when compared with DMWD. This occurs on all except the synthetic wind with gust at 55 seconds, a time previous to the ramp-in of the load relief control law. Other analysis, not shown here, reveals that the maximums associated with this wind gust will also be reduced if the gain schedule is changed to ramp in the load relief gains earlier in flight. However, this will be done at the expense of somewhat higher bending moments during the later stages of flight.

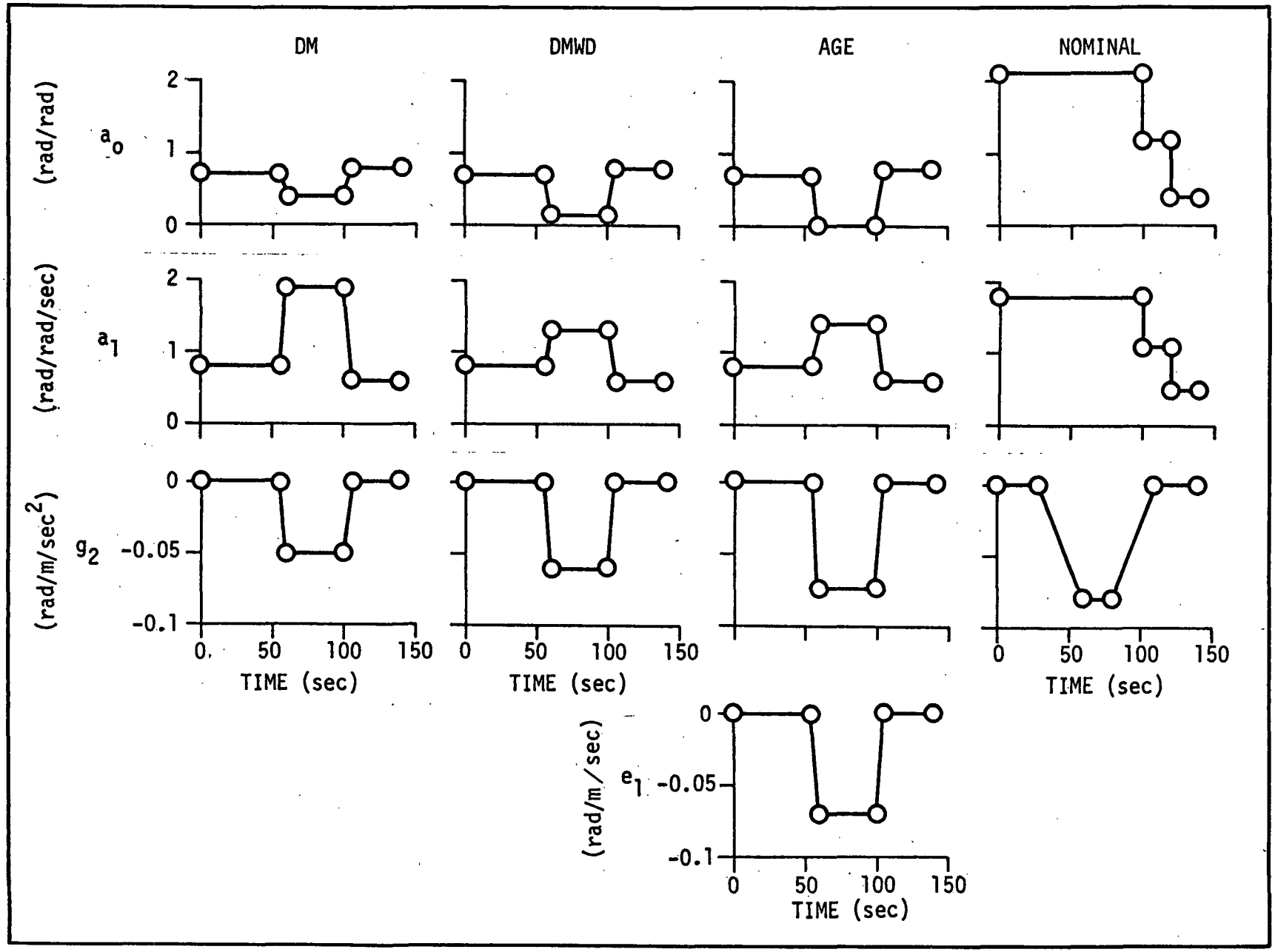

Figure 3-7. S-IB-AAP GAIN SCHEDULES FOR DM SYSTEM, DMWD SYSTEM, AGE-SYSTEM AND NOMINAL GAIN SCHEDULE

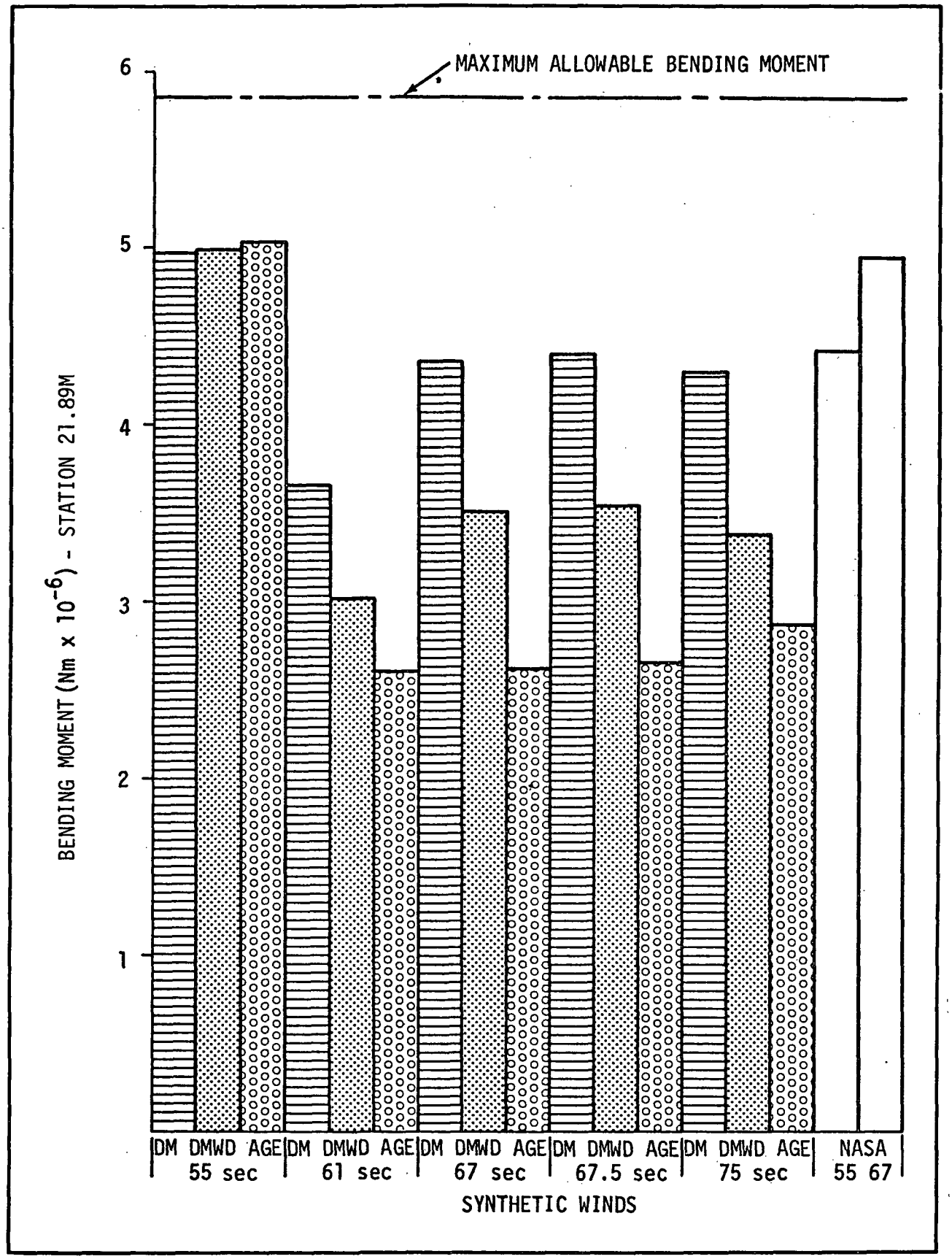

Figure 3-8. MAXIMUM BENDING MOMENTS FOR VARIOUS CONTROL LAWS FOR 5 SYNTHETIC WINDS

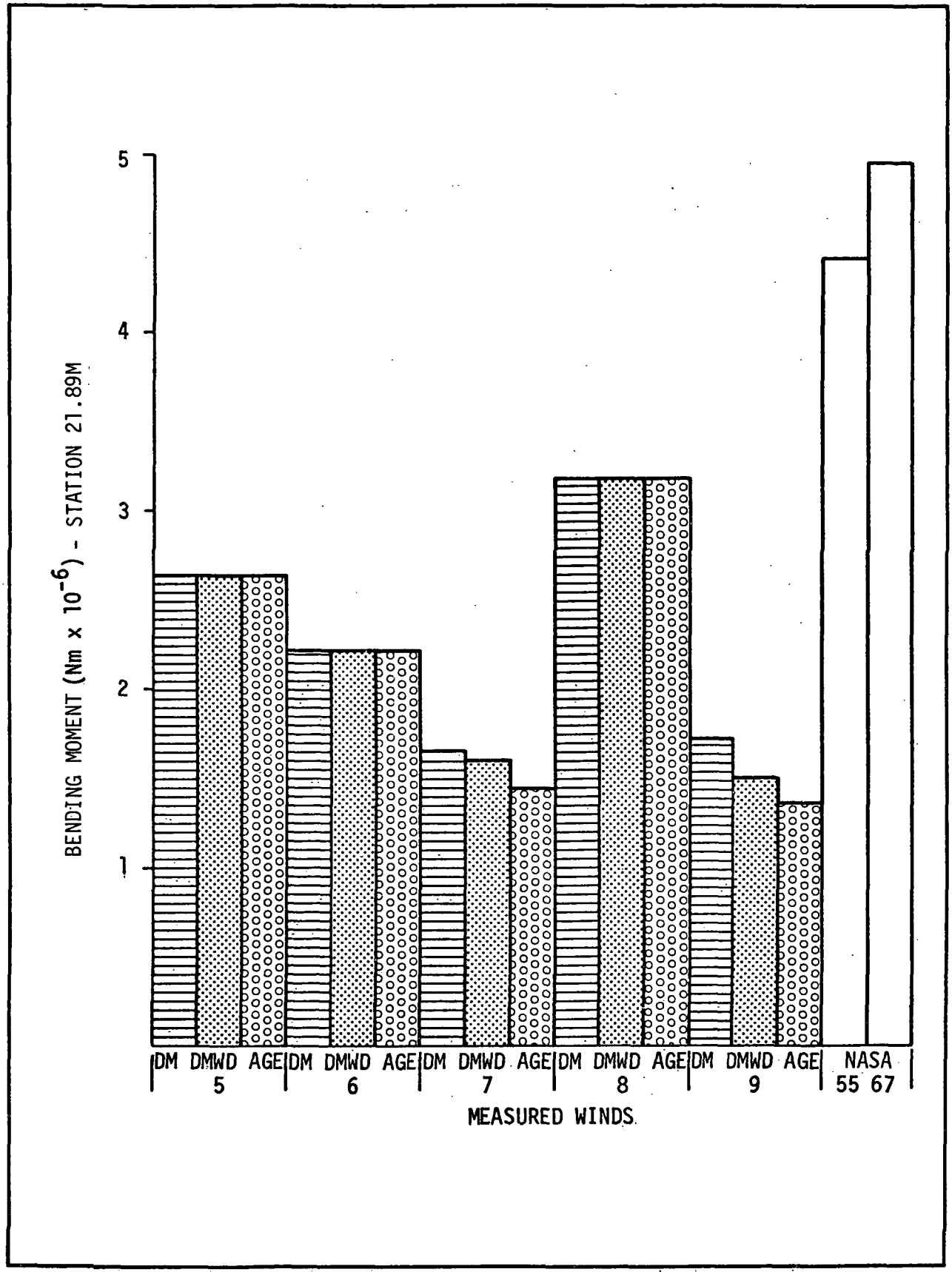

Figure 3-9. MAXIMUM BENDING MOMENTS FOR VARIOUS CONTROL LAWS FOR 5 MEASURED WINDS

The maximum bending moments for the named control laws against five measured winds are given in Figure 3-9. It can be seen from this figure that measured winds produce less severe bending moments than the synthetic winds used.

Bending moments are approximately the same except AGE is slightly lower when differences are visible. From this result and other similar results it is concluded that AGE is relatively less effective when the absolute wind magnitudes are lower and when real winds with repeated gusts and shears are considered. However AGE is never less effective than the other control laws in any wind.

3.2.4 Summary

Summarizing the results for the S-IB Wet Workshop, AGE was again shown to be the most effective load relief law. Bending moment reductions are no less than 13 percent when compared with DMWD against synthetic winds. The controllability margin is much improved when compared to the current flight controller, but DMWD gives similar results. Against the measured winds AGE again has the edge, but the improvement over DMWD is slight. However, any of the proposed systems, including the current NASA system, will handle these winds.

3.3 SKYLAB LAUNCH VEHICLE

3.3.1 Problem Definition and Approach

This vehicle, designed to launch a small space station in 1972-73, is the first to show unacceptable bending moments in the AC mode when launched against a 95 percent March synthetic wind. Even wind biasing will not give acceptable launch margins for the most severe synthetic winds. Therefore, load relief control becomes necessary on this booster stack if one is to avoid reduced launch availability.

The method of attack on this vehicle differs from the previous two in several ways.

- The simulation used is a five-degree-of-freedom (no roll) flexible body simulation of the Skylab Launch Vehicle.
- Load relief laws used are AGE and load minimum. The latter control system uses the same feedback paths as AGE but does not feedback the reference velocity (associated with e_1 gain).

- Flexible body effects are included for the first time to determine the influence of flexible body modes on the load relief capabilities of each control law under investigation.
- There are two stages in the analysis, called "sensed" and "unsensed". In the unsensed analysis flexible body motion is present in the vehicle but ideal filters are assumed, i.e., no bending motion is fed back through the control system. In the "sensed" analysis flexible body motion is felt at the sensors and the sensor signals are fed back through simple compensating filters.

As in the previous analyses the load relief control laws are used only during the period of high aerodynamic loads. As in the past this is accomplished by flying the vehicle under AC during the early flight phase then ramping the attitude gain to zero while ramping in the desired load relief gains.

Ramp durations of five seconds are used, ramp-in beginning at 45 seconds and ramp-out at 95 seconds. These times were determined by experimentation with the synthetic wind profile and the measured wind described below.

Since this program has yaw and pitch capability, two different synthetic winds were used. Both were 95-percentile profile with 99-percentile gust and shear. One wind was made to blow in the pitch plane and one in the yaw plane. It is in the yaw plane that previous analysis had shown the unacceptable loads to occur. The measured wind used in the study was measured at the AS-504 flight. It is a particularly severe wind with several major gust peaks, repeated shears, and swirls. This wind is shown in Figures 3-10(A) and 3-10(B) in pitch and yaw components. This is the worst measured wind in which a Saturn vehicle has ever actually flown.

On Skylab, the problem of vehicle drift during load relief control was addressed. In first stage flight, current Saturn vehicles use an open-loop pitch command to cause the vehicle to follow the desired trajectory. If there is no wind this commanded tilt program will satisfy the trajectory perfectly. However, AGE (and load minimum) has no provision for this since the attitude channel is open. It was decided to compensate for this by calculating a tilt rate program to satisfy the trajectory. This was done and the tilt rate program gives a satisfactory trajectory, following the nominal perfectly in the absence of wind.

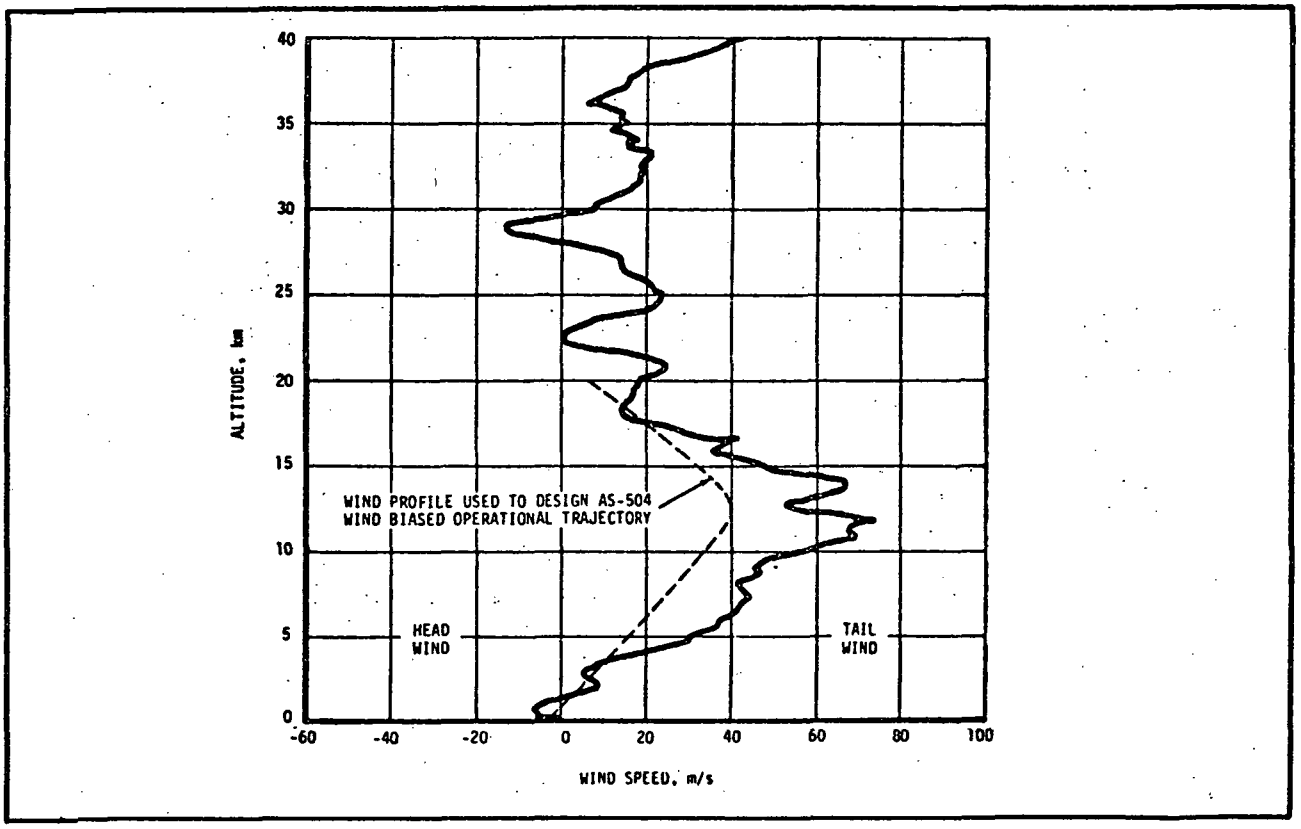

Figure 3-10A. PITCH WIND SPEED COMPONENT (W_x) AT LAUNCH TIME OF AS-504

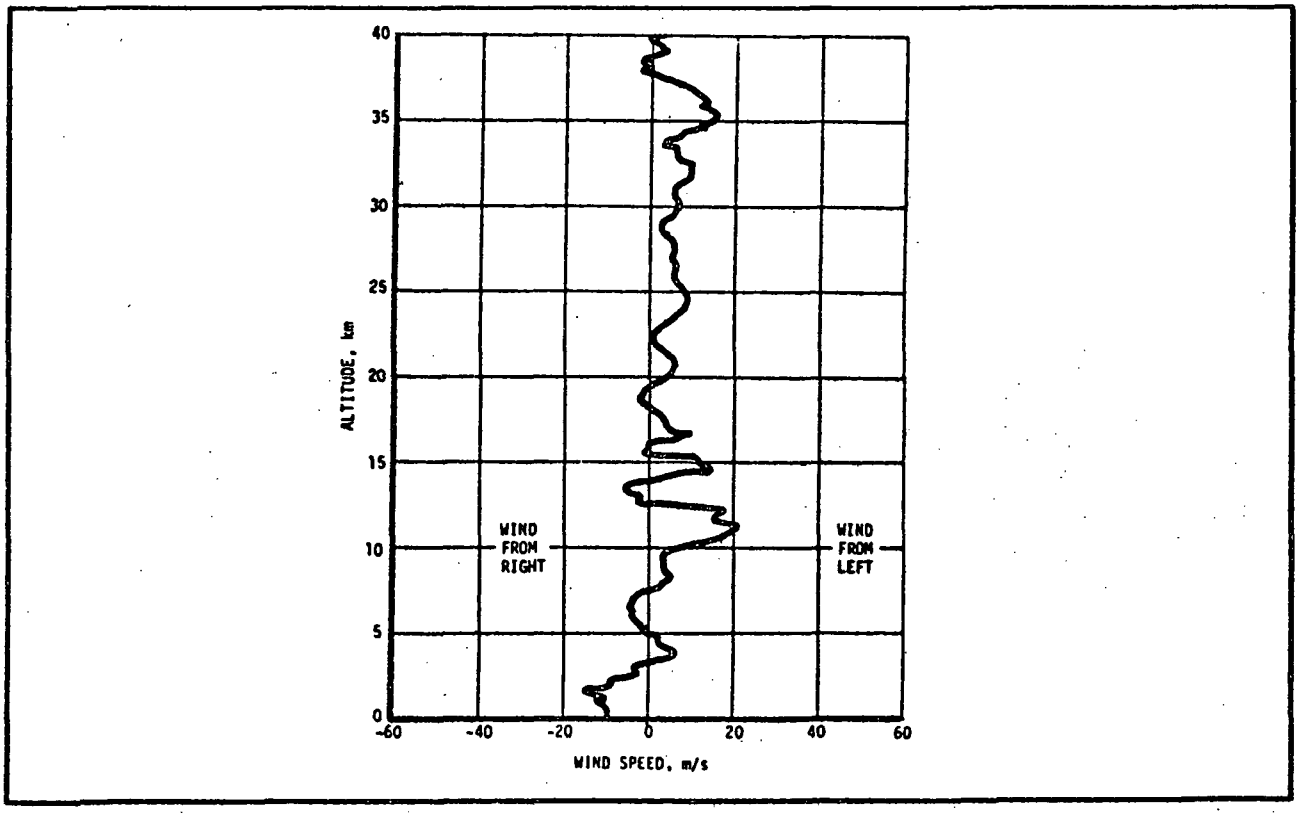

Figure 3-10B. YAW WIND SPEED COMPONENT AT LAUNCH TIME OF AS-504

3.3.2 Results of Unsensed Analysis

Most of the control comparisons are performed using unsensed flexible body modes. Bending moments are calculated at station 26.0 meters, which is toward the top of the first stage. This point is chosen since the maximum bending moment due to engine gimbal angle occurs here. The maximum bending moment due to angle-of-attack occurs at a station slightly forward of this, but the maximum total bending moment magnitude should be in this vicinity. Bending moments include the flexible body contributions in both unsensed and sensed flexible body studies.

Table 3-1 summarizes the results of the unsensed flexible body analysis for the Skylab. It can be seen that maximum bending moments are reduced 17 percent or more with AGE and 26 percent or more with load minimum. As in the past the measured wind is the most troublesome to load relief control laws. It should be noted that the flexible body bending moment contributions do not degrade the AGE load reduction capability significantly. The highest bending moments are seen in the crosswind case due to the increased cross sectional area exposed to the wind from the side direction. As usual the AGE control law is most effective on the highest loads.

In the AGE row several entries have two values. The first is the value coincident with the wind gust. The second value is that coming during the post gust buildup. As mentioned previously, this is a characteristic of AGE. In all cases bending moments are the maximum bending moments observed at any time in flight.

The load minimum control law is consistently the best performer of the three, but at the time of compilation of this table no results for load minimum had been obtained past around 90 seconds into flight. It was known that load minimum control allowed sizable trajectory and attitude divergence and the drift velocity exceeded the maximum amplifier scale. Later in the analysis, this problem was solved and it was found that the terminal drift velocity was considerably higher than AC or AGE (Table 3-2) and the attitude divergence at the end of the load minimum flight phase caused a large transient in the control system and hence a large bending moment at that time (Table 3-3). However information on the magnitude of the bending moments relative to the bending moment limits is lacking; therefore no statement can be made on the severity of these transient induced loads.

Table 3-1. SKYLAB LAUNCH VEHICLE - ACTIVE LOAD RELIEF STUDY

CONTROL	TAIL WIND - 95% SYN.			CROSS WIND - 95% SYN.			MEASURED AS504 WIND		
	α_T (deg)	β_T (deg)	BENDING MOMENT 26m	α_T (deg)	β_T (deg)	BENDING MOMENT 26m	α_T (deg)	β_T (deg)	BENDING MOMENT 26m
ATTITUDE CONTROL $a_0 = .9$ $a_1 = .7$	10.0	3.8	43.0×10^6 N-m	11.5	4.4	50.0×10^6 N-m	7.5	2.3	31.0 $\times 10^6$ N-m
ATTITUDE CONTROL $a_0 = .9$ $a_1 = .9$	10.0	3.6	41.0	11.0	4.2	48.0	8.0	2.2	30.0
LOAD MINIMUM	3.2	1.6	14.0	4.0	2.0	20.0	7.0	1.4	22.0
AC-22 AGE 212 (BEST)	3.6/6.4*	1.6	16.0	4.5/9.0	2.0	21.0	7.0/7.0	1.5/2.2	25.0

* *NOTE: Gust Time 68 sec/Post Gust Response Buildup @ Approx 80 sec*

Table 3-2. DRIFT VELOCITY (M/SEC) VS CONTROL LAW

CONTROL LAW	TERMINAL DRIFT VELOCITY
AC	50.0
AGE	-17.0
Load Minimum	-100.0

Table 3-3. PEAK BENDING MOMENTS DUE TO SYNTHETIC PITCH PLANE WIND

CONTROL LAW	BENDING MOMENT (STA 26m) AT WIND GUST (n-m x 10^{-6})	BENDING MOMENT (STA 26m) DURING LATE FLIGHT (n-m x 10^{-6})
AC	41.0	No buildup or transient
AGE	16.0	13.0
Load Minimum	14.0	23.0

This late flight, ramp-in transient is characteristic of a load minimum control law and there appears to be no action that will reduce the ramp-in ping without compromising the load relief at the wind gust. Furthermore, the terminal drift velocity magnitude is significantly larger than the AC or AGE values and it is believed probable this would impact performance of the booster. For these reasons load minimum is dropped from further consideration in this study.

3.3.3 Results of Sensed Analysis

For the sensed part of the analysis AGE is the only load relief control law used. Table 3-4 compares various responses against the synthetic pitch wind. The bottom entry is the row that gives the AGE control law with vibrations sensed and using filters that stabilize the two body modes. The filters cause some degradation in the responses as can be seen. However the degradation is considered acceptable and indeed the Intermediate-21 work in subsection 3.4 indicates that AC is more sensitive to filters than AGE. Filtered responses with AC control laws increase by a larger percentage than filtered AGE responses.

Table 3-4. RESPONSE COMPARISON FOR VARIOUS CONTROL LAWS AGAINST 95% SYNTHETIC PITCH PLANE WIND @ 67°

CONTROL	$\dot{\phi}_P$ deg/sec @ GUST	α_P deg @ GUST	β_P deg @ GUST	BM(26) N-m @ GUST	DRIFT Y_R (m) @ END CONDITION	DRIFT RATE $\dot{Y}_R$ (m/sec) @ END CONDITION
BEST ATTITUDE CONTROL $a_o = .9$ $a_1 = .9$	1.0	10.0	3.6	41.0 $\times 10^6$	3000	50.0
AGE (BEST)	2.3	3.6	1.6	16.0	-1250	-17.0
LOAD-MINIMUM	2.4	3.2	1.6	14.0	-4000	-100.0
AGE $\ddot{\eta}$ SENSED CLOSED LOOP	1.6	4.0	1.5	18.0	-300	5.0

3.3.4 Summary of Skylab Load Relief

- The AGE load relief control scheme reduces in flight loads in the Skylab launch vehicle significantly even when flexible body motion is sensed and fed back, provided suitable filters are used.
- The AGE system demonstrated its ability to handle a variety of in-flight winds and to achieve reasonable end conditions. Crosswinds produce the largest control excursions and bending moments due to the larger projected surface area of the vehicle.
- The AS-504 measured wind showed the least improvement under AGE of any wind used in this study. The ability of the AGE system to reduce bending moments caused by this wind was compromised, but bending moments caused by this wind are lower than those caused by the synthetic winds.
- The AGE control system performed better than the AC or load minimum systems where vehicle drift is concerned.

3.4 INTERMEDIATE-21 LAUNCH VEHICLES

3.4.1 Problem Definition and Approach

Intermediate-21 is a name applied to a stack consisting of the first two stages of the Saturn V launch vehicle and a payload of the same diameter (33 feet) replacing the third stage. Three payload lengths were studied. Two of them, 107 feet long and 141 feet long, are large space station modules proposed for the 1980's or late 1970's. The remaining payload is the proposed Reusable Nuclear Shuttle, 187 feet long.

The first problem facing the investigator on these vehicles is controllability. Results shown in references 1 through 3 indicate that the usual 95-percent synthetic wind causes the 107-foot payload's gimbal angle to approach or equal the current gimbal limits (5.15 degrees) and causes the 141- and 187-foot payloads' gimbal angles to exceed the limits by a substantial margin. Therefore, the controllability problem must be conquered before the bending moment problem is approached. If controllability can be established, then the bending moments can be calculated and it can be determined if the vehicles will fly without exceeding their structural limits.

As these vehicles are alike except for the length of their payloads, it was decided to perform a thorough rigid body analysis of the three configurations in order to get an idea of the effect of payload length. If no unexpected trends developed, the flexible body stage of the study would concentrate on the 141-foot payload and these results could be extrapolated to the other two payload lengths. The 141 was chosen because it was considered the most likely to reach the hardware stage.

Since the previous work has shown AGE to consistently be the most effective load relief control law, no other load relief law is considered in this section. The major remaining undesirable rigid body effect of AGE is post gust buildup. Gain tuning is attempted during the rigid body variable time analysis to relieve this problem.

After the rigid body work is complete, the flexible body math model (Figure 2-1) is implemented. This is a study to show the feasibility of an AGE control law considering flexible body effects so the analysis is performed in frozen time. The time point chosen is maximum $q\alpha$ (71 sec) which is the worst flight time for rigid body. It is considered a good assumption that if one stabilizes a control law at maximum $q\alpha$ and still obtains satisfactory performance one can repeat the process at any other flight time.

The flexible body analysis of the Intermediate-21 vehicles follows the procedure used on Skylab up to a point but several new areas of interest have been uncovered since the Skylab analysis.

From Figure 2-1 the reader can see that the body bending modes (equation (5)) were being driven by the engine alone. In reality, a significant contribution is also made by the angle-of-attack coupling, although equation (5) should be adequate to assess stability, relative modal values between the control laws may be changed by this new term. For the change equation (5) becomes

$$m_{b_i}[\ddot{\eta}_i + 2\zeta_i\omega_i\dot{\eta}_i + \omega_i^2\eta_i] + [k_E m_E Y_i(X_E) + I_E Y^1(X_E)]\ddot{\beta}$$

$$+ mK_3 Y_i(X_E)\beta + QCN_{\eta_i}\alpha = 0 \qquad (5a)$$

In the Skylab work and during the first part of the Intermediate-21 work the accelerometer sensor was located at the first and second interstage (36.6 m). For implementation reasons it was desired to examine the feasibility of locating it at the instrument unit (62.2 m on this vehicle). This is considered in this section.

3.4.2 Rigid Body Results

A wind study was performed on all three payloads, comparing AC against AGE for each payload. The family of synthetic winds has 95-percentile profiles, 99-percentile shear buildups and gusts occurring at flight times from 55 seconds to 120 seconds. Added to these is an idealization of the AS-504 measured wind to one plane. Several of these winds are shown in Figure 2-2. The results of the synthetic wind study for the 141-foot payload are shown in Figure 3-11. It can be seen that the peak α and β (variable time) occur at maximum $q^*\alpha$ for AC while the AGE control law has its β peak at maximum q (81 sec) and α peak at maximum $q^*\alpha$. This justifies the choice of 71 sec as the frozen time point for the flexible body study.

Figure 3-12 shows the peak α and β associated with each payload length at maximum $q^*\alpha$. Note the dramatic reductions in α and β which are caused by the AGE control law. Gimbal angles no longer approach the limits with the AGE control law. They are reduced 47 to 56 percent, depending on the payload length. Reductions in angle-of-attack are about the same for each payload, roughly 55 percent. Figure 3-12 points out a significant feature of AGE; i.e., the more severe the load or controllability problem the greater percentage reductions AGE yields.

Other results presented in reference 13 show that AGE reduces the α and β induced by the AS-504 measured wind to a lesser percentage than those quoted above. Angle-of-attack is reduced about 28 percent and gimbal angle is reduced from 7.5 percent to 14 percent. A 95-percentile profile reverse 99-percentile shear wind causes little problem to either AC or AGE.

The problem of post gust buildup was also attacked in this analysis. It was believed that gain tuning would eliminate or reduce this problem and that

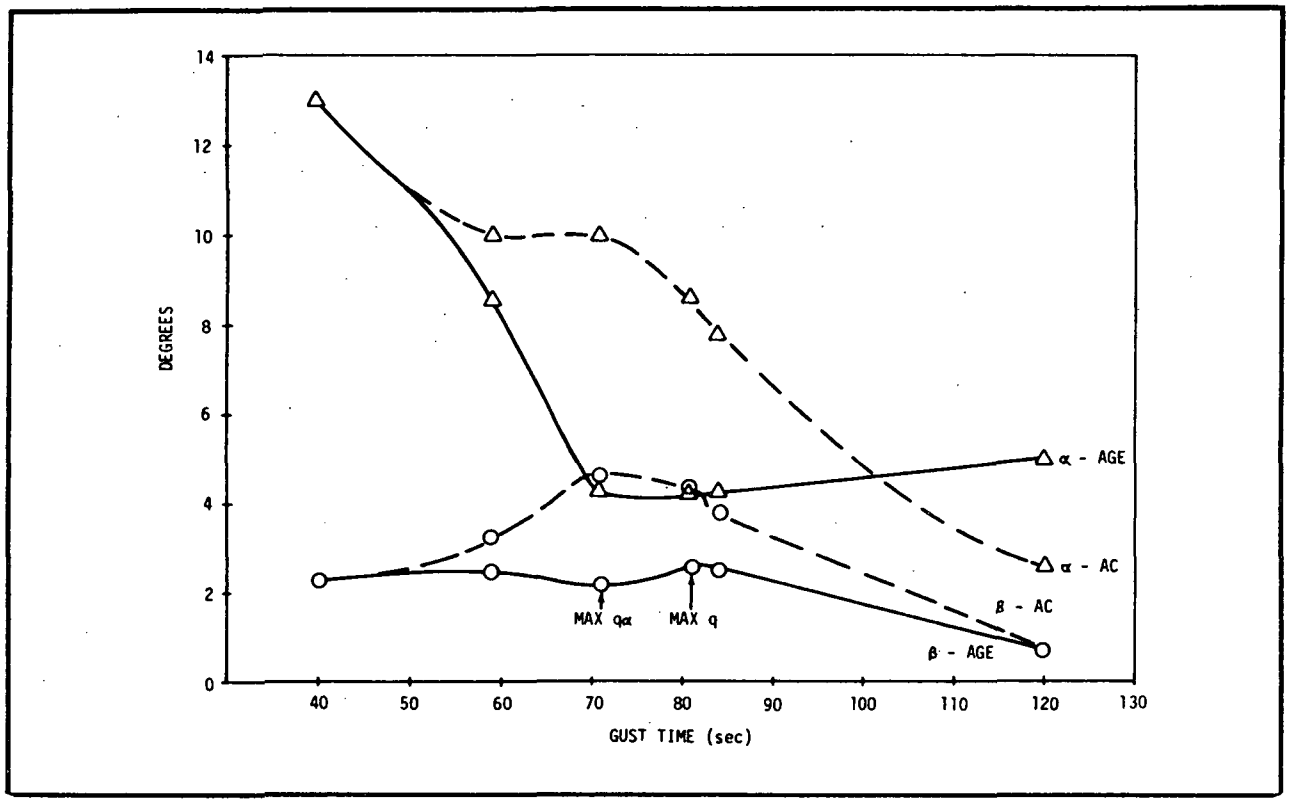

Figure 3-11. RIGID BODY VARIATION OF PEAK α, β WITH TIME OF GUST - 95% SYNTHETIC WIND, 141-FOOT PAYLOAD

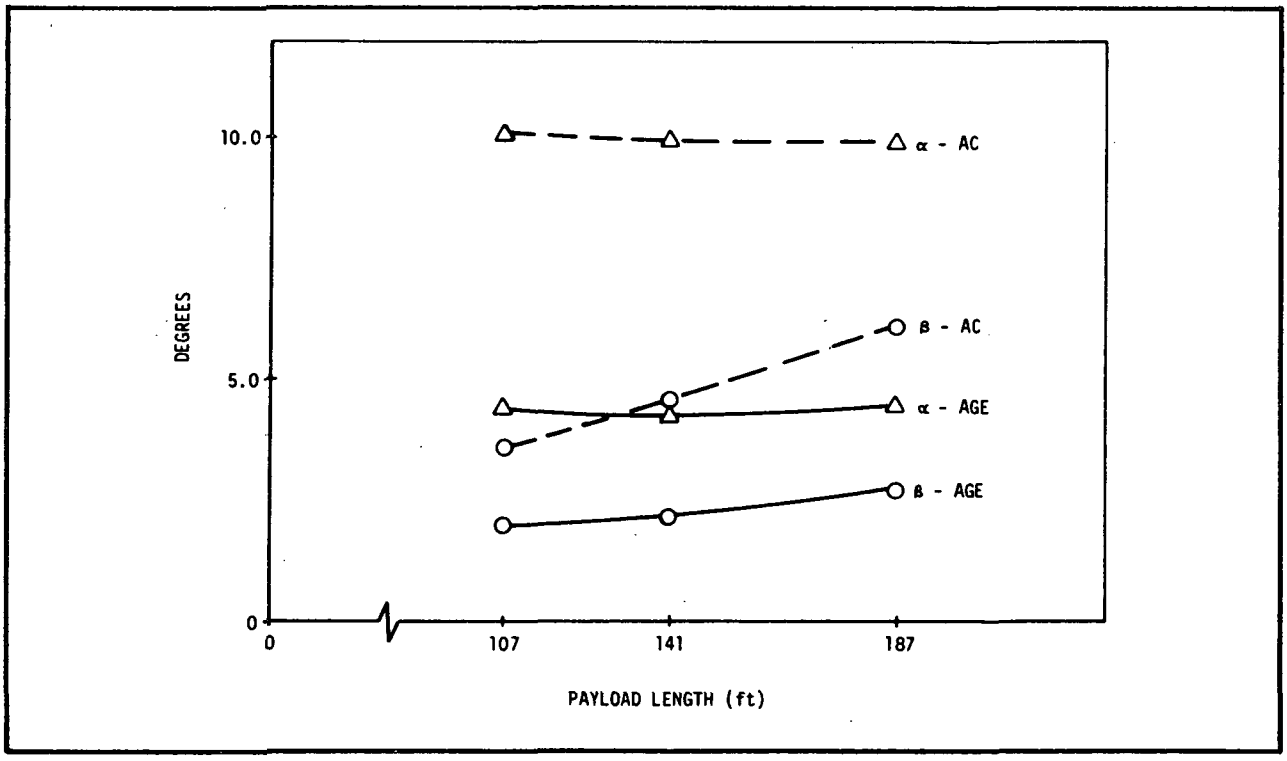

Figure 3-12. RIGID BODY α, β RESPONSES VS PAYLOAD LENGTH - GUST AT MAX Qα - 95% SYNTHETIC WIND

turned out to be a correct assumption. By using a straight line ramp for the AGE gains so that the booster's closed loop natural frequency (ω_n) and damping ratio (ζ_n) were held nearly constant as the vehicle parameters (mass, aerodynamics, etc.) were changing, it proved possible to eliminate the undesirable buildup. All the previous rigid body results used these gains. Examination of time traces in reference 11 will show that the characteristic late flight α, β (and bending moment) buildups have been eliminated.

3.4.3 Flexible Body Results

3.4.3.1 Feasibility Study. For reasons given above the flexible body analysis concentrated on the 141-foot payload at the frozen time point 71 seconds. Much of the effort on this study was in designing suitable filters at this time point. At this point guidelines for the study gave the accelerometer location at 36.6 meters. The math model was the one shown in Figure 2-1.

Reference 13 shows the results of this study. Root-locus and Nyquist programs established the stability of each payload and a hybrid simulation (2-D) was used to verify the results of the stability programs. The set of filters designed for the 141-foot payload proved to be usable for the 107- and 187-foot payloads. Gain and phase margins can be found in reference 13. AGE margins are lower than AC throughout. Angle-of-attack and gimbal angle maximums continued to show the same dramatic reductions with AGE as they showed in the rigid body study. It should be emphasized that AGE filters are low order preliminary and designed only to show feasibility. Improvements in the gain and phase margins should be possible with carefully designed, higher order filters.

3.4.3.2 Angle-of-Attack Coupling. As described in subsection 3.4.1 the effect of α on the bending modes is an important problem. When the math model is so altered, the bending mode accelerations are increased sharply with both AC and AGE. The net result is that AC and AGE have about the same modal acceleration magnitude (ref. 13).

3.4.3.3 Accelerometer at IU. Without changing the simple second-order filters of subsection 3.4.3.1, the accelerometer was relocated to the IU of this vehicle.

The modes remained stable but the relative magnitudes of $\ddot{\eta}_1$ and $\ddot{\eta}_2$ were changed since the first mode influence coefficient at the IU has about half the magnitude there as it does at the interstage (ref. 2). Slight oscillation was displayed by some of the rigid body variables but this was attributed to the use of the filters designed for an accelerometer mounted at the interstage instead of the IU.

3.4.3.4 Parametric Responses. Figures 3-13 and 3-14 show the peak α and β values of all three payloads with all these past assumptions in force. Note the high reductions in α and β (about 67 percent for the 141-foot payload). These results were taken from the 2-D hybrid simulation with flexible body modes, frozen coefficients, non-linear aerodynamics, and the accelerometer located at the IU.

3.4.3.5 Bending Moments. To get some idea of the bending moments caused by the α, β values, Figure 3-15 has the bending moments along the vehicle (141-foot) for AC and AGE. For comparison it also has the bending moment limits referenced on the graph. The bending moment limits were obtained for the Saturn V and they terminate around 2400 inches since no limits are known for the 141-foot payload substituted for the present S-IV third stage.

The AGE control law reduces the bending moment by as much as 70 percent, but does not conclusively show the bending moments will not exceed the limits. In addition, flexible body contributions to bending moment (equation (1)) are not included for lack of data. They usually add about 10 percent to the value (ref. 9). (However in section 3.4.3.2 it was established that AC and AGE have about equal $\ddot{\eta}_1$ so they will not change the relative values of the bending moments.) On the other hand these are frozen time results; 20 to 30 percent conservative. Furthermore, the bending moment limits are for a manned vehicle (1.4 factor of safety) whereas the Intermediate-21 will be unmanned (1.25 factor of safety) (ref. 10). It is believed the net results would let the vehicle stay within the bending moment limits, but the problem needs further study.

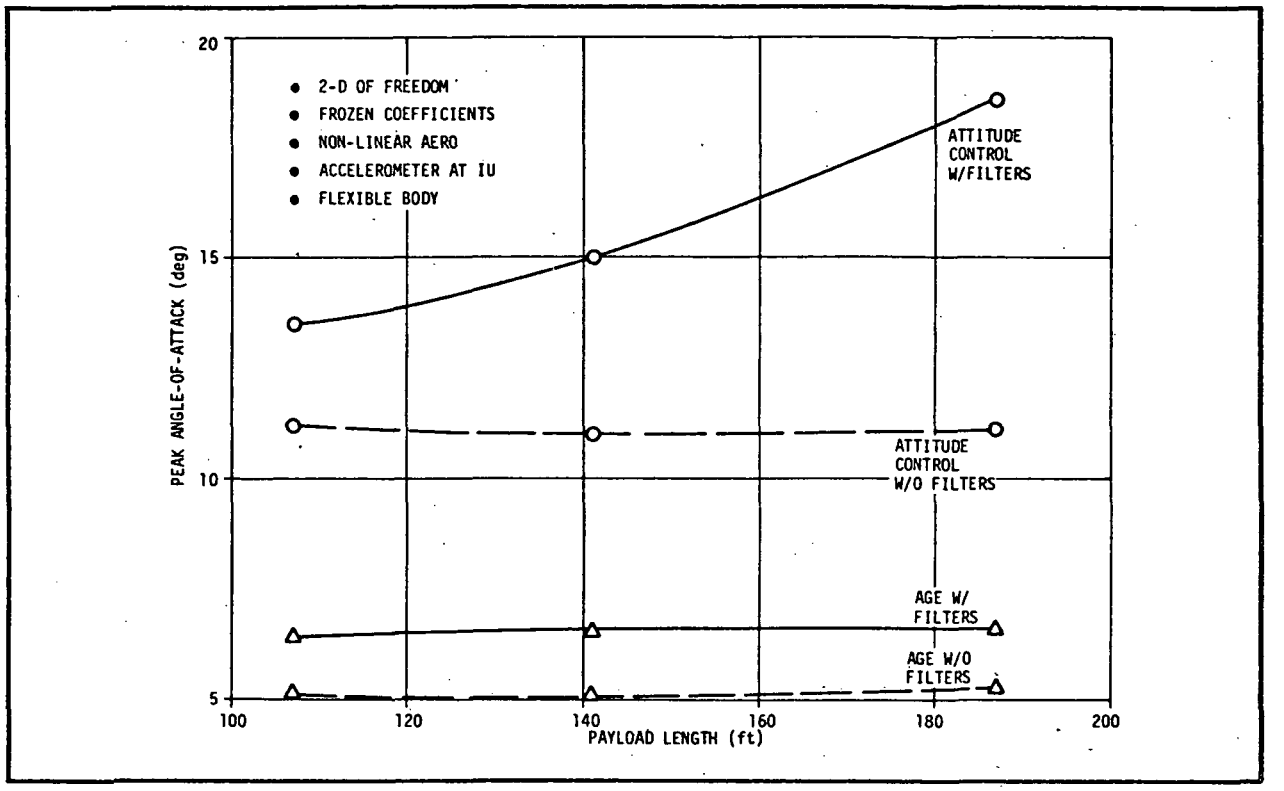

Figure 3-13. ANGLE-OF-ATTACK VS PAYLOAD LENGTH

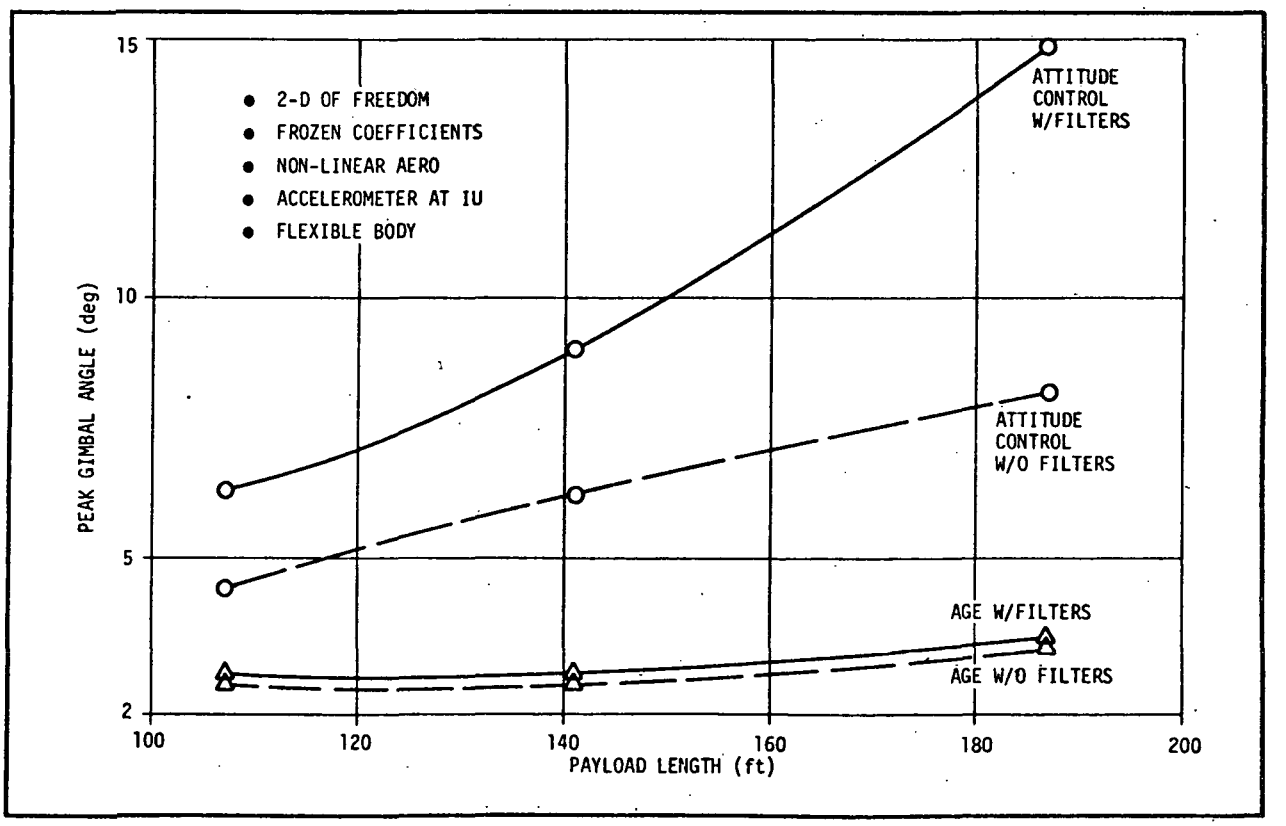

Figure 3-14. GIMBAL ANGLE VS PAYLOAD LENGTH

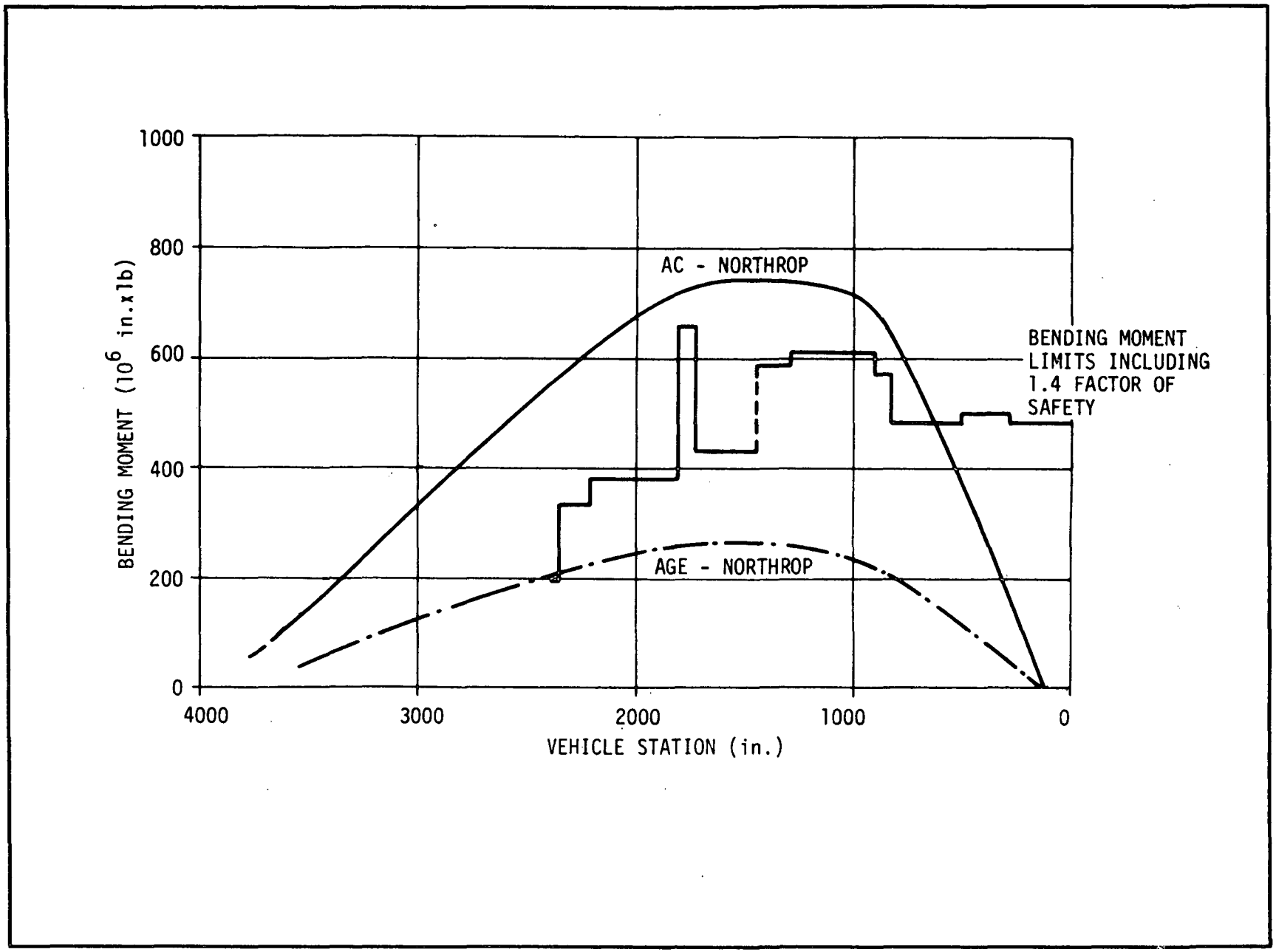

Figure 3-15. BENDING MOMENT COMPARISONS - 141-FOOT PAYLOAD

3.4.3.6 Typical Responses. To illustrate the comparative effects of AC and AGE control laws on a vehicle with nonlinear aerodynamics, simplified filters and two flexible body modes driven by aerodynamics and engines, Figures 3-16 and 3-17 are included. These responses are taken from frozen time. They show the sharp reductions in α and β that AGE affords. The AGE control law allows the heading error (ϕ) to diverge from zero (into the wind) as it encounters the wind. This is the mechanism that permits the vehicle to incur lower bending moments during flight. By contrast ϕ is away from the wind during AC flight. Note that the bending accelerations ($\ddot{\eta}_i$) are about equal in the first mode but AGE accelerations are higher in the second mode.

3.4.4 SUMMARY

3.4.4.1 Conclusions.

- On any of the Intermediate-21 configurations AGE reduces bending moments by more than one-half the corresponding AC value.
- Under AGE control none of the configurations' gimbal angles exceed the current limits (5.15 deg). However, the 141-foot and 187-foot payloads do exceed 5.15 degrees gimbal angle with AC control.
- Flexible body effects on the accelerometer sensor are controllable by simple filters. Stability margins are lower than those obtained by an AC control law.
- Flight path drift and α, β post gust buildup can be controlled by gain tuning coupled with a path velocity feedback.

3.4.4.2 Recommendations.

- Further filter and stability work should be conducted with the accelerometer at the IU.
- Additional effort is required to define filters to achieve best stability margins for all flight times during first stage burn.

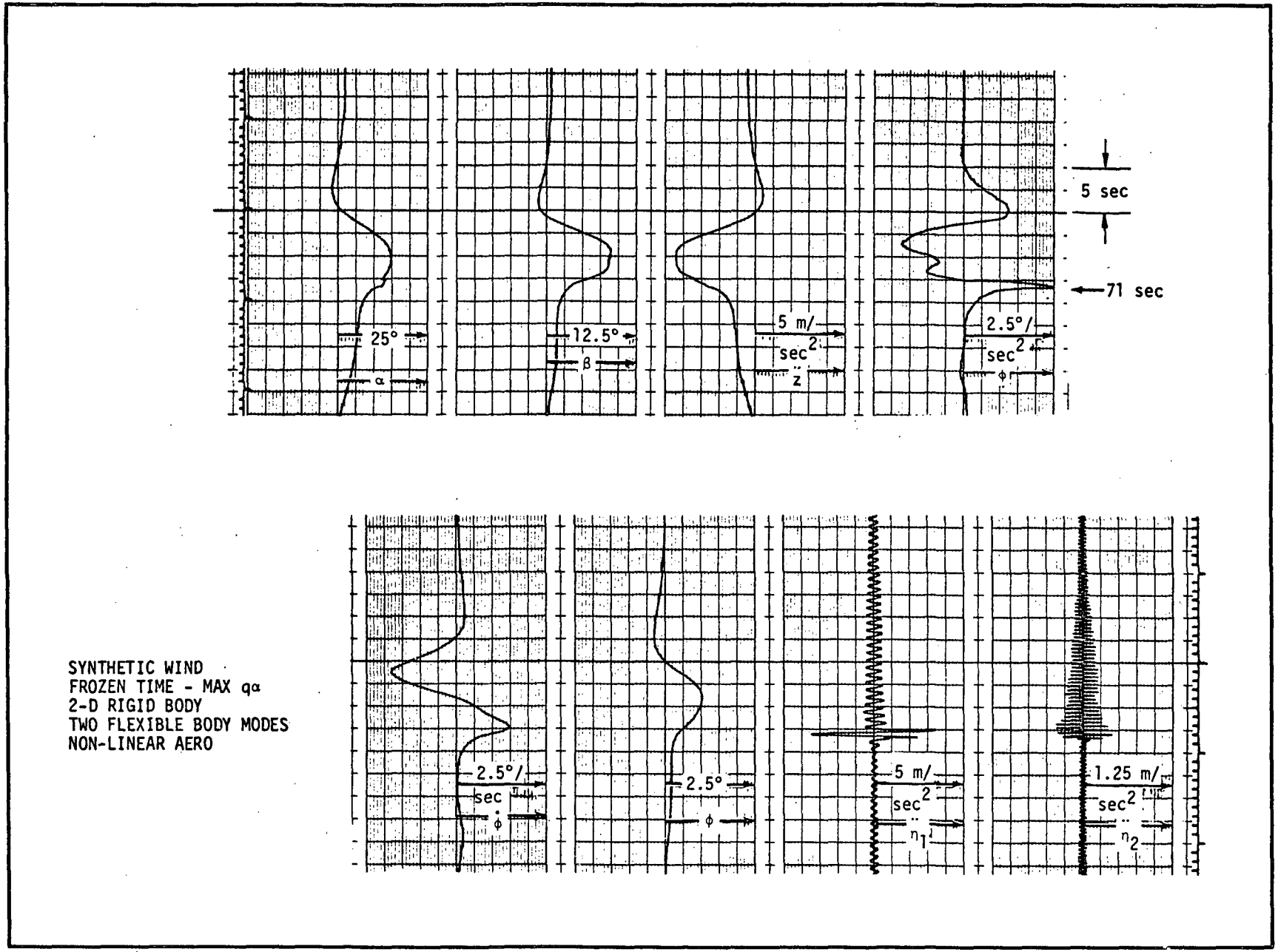

Figure 3-16. AC WITH α-MODAL [(141-FOOT)] EXCITATION - FULL BOEING SIMPLIFIED FILTERS

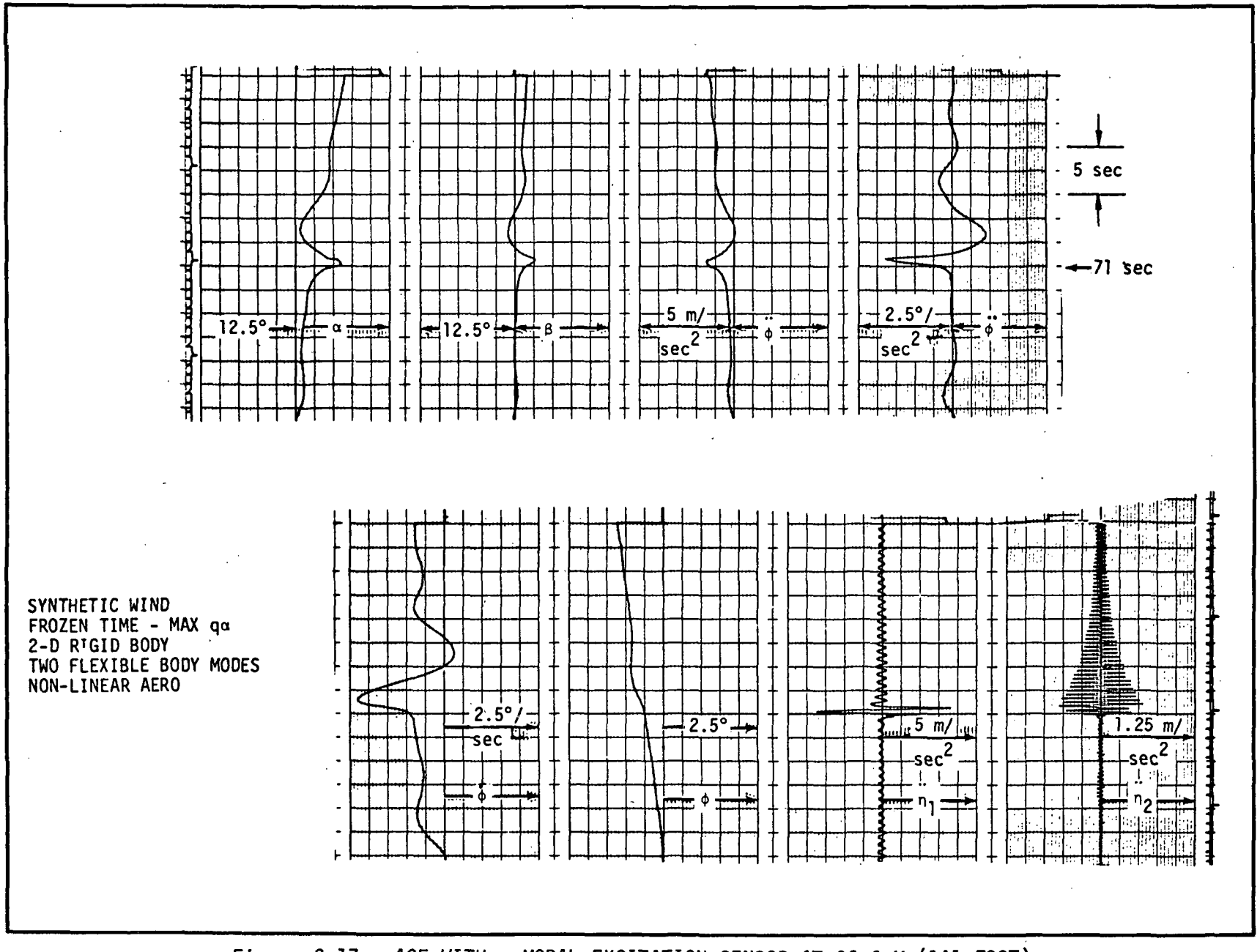

Figure 3-17. AGE WITH α-MODAL EXCITATION SENSOR AT 36.6 M (141-FOOT)

Section IV

OVERALL LOAD RELIEF CONCLUSIONS AND RECOMMENDATIONS

4.1 CONCLUSIONS

- Bending moments are lower on every configuration when an AGE control law is used. When compared with the baseline AC law reductions are typically 10-30 percent with measured winds and 30-60 percent with synthetic winds. It is believed that the key to the success of AGE lies in elimination of the preprogrammed attitude command profile.
- Drift and drift rate are lower under AGE control than under the AC control.
- Severe ramp transients and post-gust buildups can be eliminated by proper gain choices.
- Measured winds cause lower loads than the worst case synthetic wind but AGE is less effective in reducing loads caused by measured winds.
- An AGE control law will function just as well in reducing bending moments when flexible body effects are considered. However gain and phase margins are lower with the simplified filters. An increase in the order of the filters should provide adequate margins for the AGE control law.

4.2 RECOMMENDATIONS

- Additional work should be directed toward flexible body problems, especially filters. Filters are needed that will give suitable responses and stability margins and be good throughout first stage flight.
- Since the alpha meter can give equivalent rigid body load reductions a study should be made to determine the trades present between acceleration and angle-of-attack feedbacks. Problems associated with hardware qualification, location, performance and flexible body interactions need consideration.
- A cost analysis is needed to compare cost of control system modifications against cost of structural modifications for beefup of the booster and against launch limitations and turn around expenses.
- Reliability of the sensors involved should be compared. Another related area of future study is engine failure capability.

Section V

REFERENCES AND BIBLIOGRAPHY

1. The Boeing Company, "Design Data Report - Int-21 Launch Vehicle with MDAC Phase II Payload (107-Foot Long - Clean)", Attachment to Memo 5-9406-INT-21-27, July 24, 1970.

2. The Boeing Company, "Design Data Report - Int-21 Launch Vehicle with MDAC 141-Foot Payload Configuration", Attachment to Memo 5-9406-INT-21-27, July 24, 1970.

3. The Boeing Company, "Design Data Report - Int-21 Launch Vehicle with MDAC Reusable Nuclear Shuttle (RNS) Payload, Attachment to Memo 5-9406-INT-21-27, July 24, 1970.

4. Chichester, D. E., "Application of Saturn V Intermediate Launch Vehicles to Space Station/Space Base Missions", Volume 4 - Controls, The Boeing Company, 5-9410-H-087-4, October 30, 1970.

5. The Boeing Company, "Digital Program BHA0030-D Saturn V/S-IC Flight Dynamics" (Digital Computer Program).

6. The Boeing Company, "Application of Saturn V Intermediate Launch Vehicles to Space Station Missions - Final Technical Report", D5-15804-2, August 10, 1970.

7. Mayeaux, H. J., "Load Relief Control Law Investigation and Data Report for Saturn V/Apollo Launch Vehicle", Northrop-Huntsville, TR-795-8-419, September 1968.

8. Kiefer, H., "Rigid Body Load Relief Study For S-1B-AAP Configuration (Wet Workshop)", Northrop-Huntsville, TR-795-9-653, November 1969.

9. Cerny, O. P., Foster, L. W. and Sharp, J. B., "Load Relief Attitude Control of the Skylab Launch Vehicle", Northrop-Huntsville, TR-795-795, October 1970.

10. Lane, L. G., "Intermediate-21 Launch Vehicle Preliminary Description For Phase B Space Station Design", The Boeing Company, D5-15583, August 22, 1969.

11. Sharp, J. B., "Intermediate-21 Rigid Body Response Study", Northrop-Huntsville, 7951-70-30, August 27, 1970.

12. Rheinfurth, M., "The Alleviation of Aerodynamic Loads on Rigid Space Vehicles", Technical Memorandum X-53397, George C. Marshall Space Flight Center, Huntsville, Alabama.

13. Sharp, J. B., "Intermediate-21 Load Relief Attitude Control", Northrop-Huntsville, TR-795-895, March 1971.

14. Livingston, J. M. and Redus, J. R., "Load Reducing Flight Control Systems for the Saturn V with Various Payloads", AIAA Paper #68-843, August 1968.

15. "Redefinition of Saturn IB Synthetic Wind Profile", MSFC Memo R-AERO-Y-66-65, September 10, 1965.

16. "FPS-16 Radar/Jimisphere Wind Data Measured at the Eastern Test Range", NASA TMX-53290, December 22, 1965.

DISTRIBUTION

S&E-ASTR
Mr. Moore
Dr. Seltzer
Mr. Scofield
Mr. Brooks
Mr. Wojtalik

S&E-ASTN
Mr. Heimburg
Mr. Isbell
Mr. Fuhrmann
Mr. Zagrodsky

S&E-CSE
Dr. Haeussermann
Mr. McKay
Mr. May
Mr. Price

PD
Mr. Palaoro
Mr. Pedigo

S&E-P
Mr. Wiley

S&E-COMP
Mr. Prince

S&E-AERO
Dr. Geissler
Mr. Horn
Dr. Lovingood
Mr. Ryan
Mr. Rheinfurth
Dr. Worley
Mr. Mowery
Mr. Livingston (5)
Mrs. Hightower
Mr. Lindberg
Mr. Baker
Mr. W. Vaughan
Mr. Dahm
Mr. Sims

Manned Spacecraft Center
Houston, TX 77001
Attn: Mr. Kennedy, Code EG13
Mr. Cheatam, EG2
Dr. Cox, EG2
Mr. Redd, EX2

Mr. Brent Creer
210-9
NASA-Ames Research Center
Moffett Field, CA 94035

Goddard Space Flight Center
Greenbelt, MD 20771

NASA-Flight Research Center
P. O. Box 273
Edwards, CA 93523
Attn: Mr. D. Deets
Mr. S. Gee, R

Kennedy Space Center
Kennedy Space Center, FL 32931
Attn: Mr. R. Smith, FR-A

NASA-Langley Research Center
Hampton, VA 23365
Attn: Mr. W. M. Moore, 490

NASA Hdqs.
Washington, DC 20546
Attn: Mr. T. Michaels, REG
Mr. R. Livingston, MTG
Mr. Carley, MHE

Northrop Corp.
Electro-Mach. Div.
P. O. Box 1484
Huntsville, AL 35807
Attn: Mr. Sloan
Mr. Echols
Mr. Sharp (10)

Convair Airspace Div.
General Dynamics Corp.
P. O. Box 1128
San Diego, CA 92112
Attn: G. R. Griedman, Mail Zone 585-00
A. W. Nelson, Mail Zone 585-00

Air Force Flight Dynamics Laboratory
Wright-Patterson AFB, OH 45433
Attn: Mr. Westbrook, FDCC
Mr. Blatt, FDCL

The Boeing Company
Southeast Div.
220 Wynn Dr. N.W.
Huntsville, AL 35807
Attn: Mr. D. E. Chichester
Mr. W. E. Rowe

Lockheed Missile & Space Co.
P. O. Box 1103
West Station
Huntsville, AL 35807
Attn: Mr. Trautwien
Mr. Conner

A&TS-MS-IL (8)

Scientific & Technical Information
Facility (25)
P.O. Box 33
College Park, Md. 20740
ATTN: NASA Rep (S-AK/RKT)

A&TS-MS-IL (6)
A&TS-MS-IP (2)
A&TS-MS-H
A&TS-TU (6)